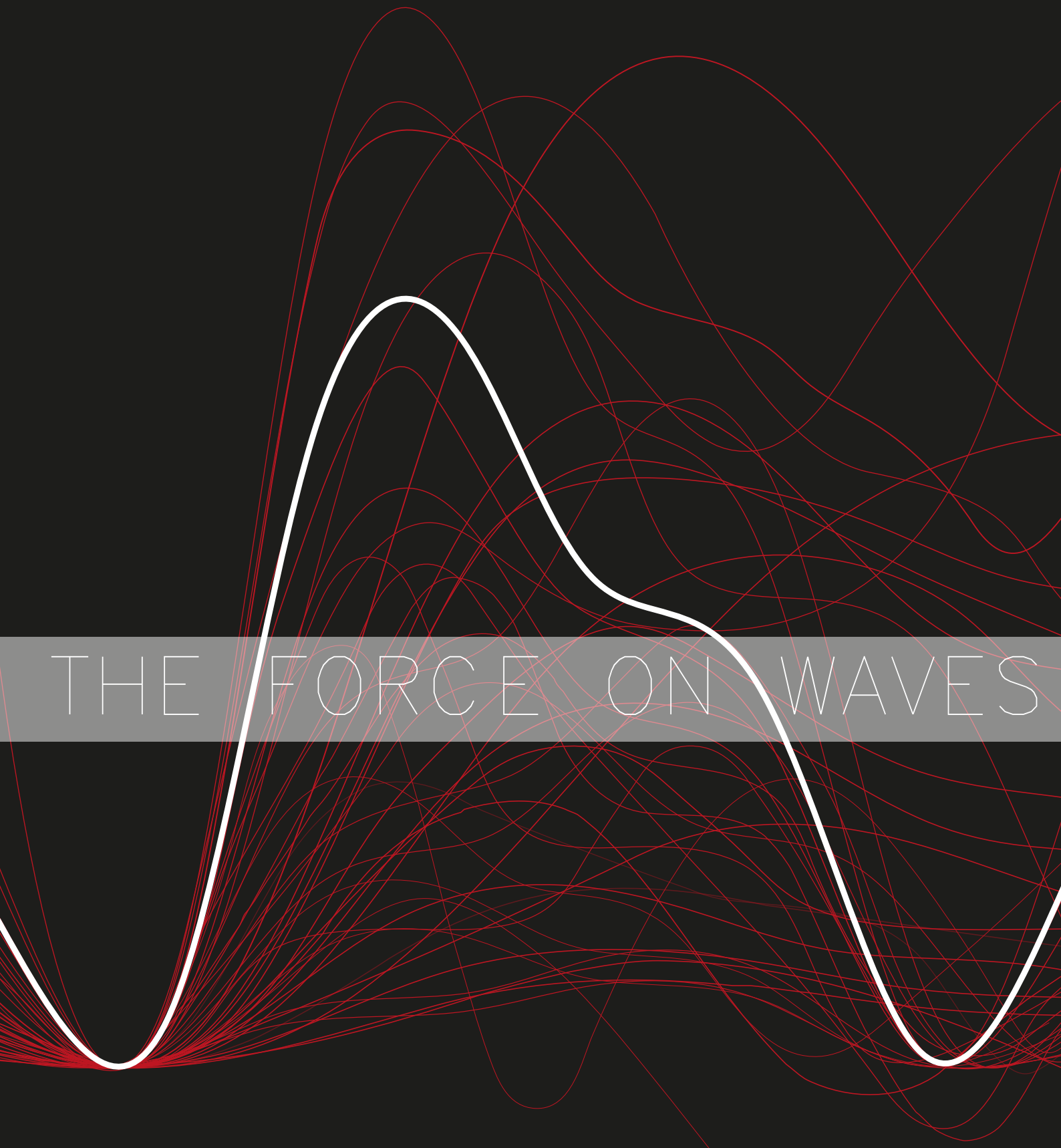

THE FORCE ON WAVES

Signal robustness dependency on sensor contact force in a novel photoplethysmography-based multi-purpose sensing device

M. Adriaanse

TU Delft

Signal robustness dependency on sensor contact force in a novel photoplethysmography based multi-purpose sensing device

By:

Michiel Adriaanse
4080475

In partial fulfillment of the requirements for the degree of

Master of Science
in Biomedical Engineering
Medical Instruments and Medical Safety

At the Delft University of Technology
Public defense will take place on Wednesday, *June 12th*, *2019* at 13:00
Instruction room A (Leonardo da Vinci) of the Delft University of Technology

Supervisors:	dr. ir. Arjo Loeve dr. ing. Marit van Velzen
Thesis Committee:	prof. dr. Jenny Dankelman dr. ir. Arjo Loeve dr. ir. Matthijs Langelaar

“Technology is the evolution of evolution”

Preface

Na praktisch mijn hele leven op school te hebben gezeten is het na het inleveren van deze thesis toch echt klaar met de pret, dus ik ga het kort houden. Afgezien van alle tegenslagen die bij onderzoek doen horen heb ik met heel veel plezier aan mijn grote masterprojecten gewerkt. Tijdens mijn stage was het weliswaar beter weer, maar tot in de diepte een project induiken heeft me doen beseffen dat ik dingen gewoon graag op de moeilijke manier doe, wat me vaak tegenwerkt, maar dat het ook wel eens helpt om niet ergens zo makkelijk mogelijk van af te willen zijn. Of zo snel mogelijk, gezien mijn studietijd. Ik ben tevreden met het resultaat wat ik uit mijn onderzoek heb weten te wringen, ookal kan ik zeer kritisch zijn over hoe dat is gebeurd. Ze zeggen niet voor niks dat het een leertraject is en als het makkelijk zou zijn geweest had het wel een bachelor geheten.

Het voelt gek om dit in het Nederlands te schrijven na bijna anderhalf jaar al met Arjo en Marit in touw te zijn geweest voor het opzetten van Engelse documenten. Ik wil ze langs deze weg dan ook enorm bedanken voor overkoepelend de begeleiding, maar meer specifiek de steun, feedback, brainstorms, pubquizzes en de hulp bij het academish zo succesvol mogelijk maken van de afronding van mijn studiejaren. Nasiem, Toten, Klup, Max, enorm bedankt voor jullie steun, expertises, en vooral gezonde en ongezonde kritiek en ontspanning tijdens deze periode. Kelsey, thank you so much for all the positive reinforcement, caring words and help with my English during the last 7 months, I hope there are many, many to follow. En als laatst maar zeker niet het minst Pap en Mam (het begint wel een beetje een acceptance speech te lijken voor de oscars zo), ook jullie onvoorwaardelijke steun heeft me er doorheen geholpen. Niet alleen de laatste paar maanden maar de afgelopen 26 jaar.

Als ik aan de lezer ook maar een fractie van plezier mag wensen in het lezen van deze thesis dan wat ik heb gehad in het uitvoeren van dit onderzoek dan zal het in een zucht uit zijn.

Michiel

Thesis contents

Preface

Signal robustness dependency on sensor contact force in a novel photoplethysmography-based multi-purpose sensing device **Page 1-16**

- Introduction and background Page 1-3
- Materials Page 3-5
- Methods Page 5-9
- Results Page 10-13
- Discussion Page 14-16
- Conclusion Page 16

Appendix A – Theoretical background

Appendix B – Statement of requirements and preferences

Appendix C – FA-MPA Design process

Appendix D – Technical documents

Appendix E – Experimentation documents

Appendix F – Future recommendations

Signal robustness dependency on sensor contact force in a novel photoplethysmography-based multi-purpose sensing device

M. Adriaanse – TU Delft

Abstract

A new photoplethysmography-based device called the Multiphotodiode Array (MPA) was validated to successfully measure the PWV in the vasculature of the distal phalanx of healthy subjects. It comprises an array of photodiodes and an array of opposing LEDs to detect blood volume changes due to the passing pressure pulse wave in the vasculature of the distal phalanx of the index finger. This study aimed to discern how the signal robustness of a novel modular sensor based on the technology of the MPA is dependent on the contact force between the vascularized tissue and the sensor surface. PWV data was collected as the distal phalanx of the left index finger from 26 subjects was placed on the Force Alterable-MPA (FA-MPA). Contact force was altered by placing differing weights (0-300g, 50g increments) on top of the phalanx using a linear stage. Contact force was determined as weight measured by a scale underneath the FA-MPA. PWV and weight data was collected from a total of 182 measurements. Measurements were pooled in 8 weight groups between 0 and 400g at increments of 50g according to the weight that was measured during that measurement. PWV data per weight group was analyzed for three characteristics: 1. Pulse Wave Quality Ratio (PWQR); 2. PWV variance; 3. Realistic and non-negative values for PWV. ANOVA of PWQR resulted in a significant effect between weight groups (p = 6.91E-7). Further qualitative judging of data resulted in the recommendation to thoroughly redesign the FA-MPA for structural and electrical integrity and measurement protocol for elimination of movement and placement artifacts and to reiterate the experiment for the contact force range of 1.96 to 4.43N.

Keywords: photoplethysmography, pulse wave velocity, contact force, variance, pressure pulse wave, signal robustness, photodiode, artifact

Introduction and background

Cardiovascular diseases (CVD) are the number one cause of mortality worldwide and most causes of CVDs are related to an increase of stiffness of the arterial wall, also seen as a loss of compliance, called arterial stiffening [2-4]. The arterial compliance is the capability of the artery to expand and contract due to pressure changes inside the artery [5]. A compliant arterial wall helps attenuate the systolic blood pressure inside the artery by expanding, after which the subsequent contraction of the artery wall propels the blood forward during diastole, aiding in a more continuous flow of blood rather than a purely intermittent one [6]. When arterial compliance decreases, the pressure pulse wave (PW), which is caused by the systole and is comparable to a sound wave, has a higher amplitude and moves more quickly through the artery [3, 7, 8]. This propagation speed is called the Pulse Wave Velocity (PWV).

The PWV is directly related to the arterial compliance by the Moens-Korteweg equation (Eq. (1)) where: E_V is the incremental elastic modulus, a measure of a material's elasticity, of the vessel wall; h_V is the vessel wall thickness; r_V is the vessel radius; ρ_{blood} is the density of the blood [5].

$$PWV = \sqrt{\frac{E_{inc,vessel} \cdot h_{vessel}}{2 r_{vessel} \cdot \rho_{blood}}} \; [m/s] \qquad \text{Eq. (1)}$$

Determining the PWV is considered the gold standard for determining arterial stiffening and can be measured using the technique of Photoplethysmography (PPG) [8-10]. PPG is an optical measurement technique with which changes in blood volume in a tissue can be detected [11]. PPG sensors comprise a light source (most often light emitting diodes (LED)) and an opposing light sensor (most often photodiodes (PD)) which are placed over a vascularized tissue (Figure 1). An increase of blood volume in a tissue decreases the transmissibility of red, near infrared and green light in the tissue, making it possible for a photodiode to detect blood volume changes in the tissue and 'see' the expansion of the artery due to the PW. This process is visualized in Figure 1 [11].

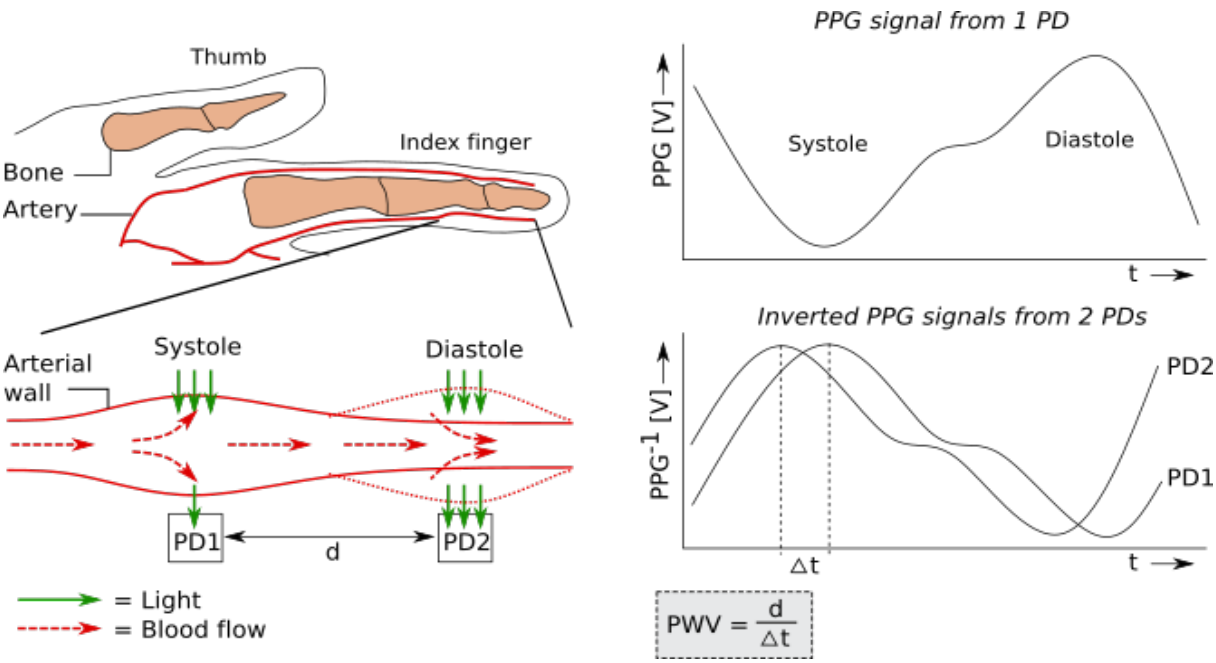

Figure 1 - Schematic representation on how the PWV is determined in the proper palmar digital artery (PPDA). Top Left: Palmar view of the left index finger and thumb. Bottom left: Close-up of the propagation of the pressure wave through the artery, d is the distance between two adjacent photodiodes. Top right: Visual representation of the PPG signal retrieved from one photodiode (PD). Bottom right: Inverted PPG signals from 2 photodiodes, showing the pulse wave (PW) waveform. Δt is the temporal difference between the PWs.

The PWV is determined by comparing the arrival times of the PWs in two locations and then calculating the PWV over the distance between these locations. Although widely available, techniques used to determine the PWV at these locations bear several disadvantages. Systematic errors in PWV calculation may be caused by discrepancies between measured PW travel distance and actual travelled distance by the PW due to the unknown precise orientation of the cardiovascular system. Also, the need for extra signal generation, for example ECG, and a specialized operator to accurately place the sensors and process the data from these signals makes the current PWV determination techniques expensive and time-consuming. Lastly, discomfort due to placement of sensors in uncomfortable locations.

In 2017, a novel PPG-based device was developed by van Velzen et al., the Multiphotodiode Array (MPA) [12]. The MPA comprises an array of 16 photodiodes and an array of 2 red and 2 infrared LEDs which are placed on opposite sides of vascularized tissue. Each photodiode in the array acts as an independent PPG-sensor, from whose signal the arrival time of the PW in the vascularized tissue can be determined. The PWV can subsequently be determined from the temporal difference between these arrival times and the distance between the photodiodes. The MPA was clinically tested on the distal phalanx of the index finger and found to be able to accurately determine the PWV in the proper proximal digital artery (PPDA), as shown in Figure 1 [1]. However, the use of the MPA was paired with some measurement artifacts, one of which was a dependency of signal robustness on the depth with which the tissue of the distal phalanx was clamped by the MPA, the ‘indentation depth’. Figure 2 shows an excerpt of PWV data from van Velzen, which shows that the robustness of the PWV determination greatly differs for different indentation depths and between two subjects. Wrongfully determined PWV values could completely negate the viability of a device used for PWV determination in the distal phalanx. It is therefore necessary to investigate what causes these artifacts, as to be able to mitigate them in the future.

Because the ‘optimal indentation depth’ differs between two subjects, it is thought that the signal robustness depends on the contact force between the MPA and the tissue and not the clamping depth. This study aims to investigate the effect of the contact force between a PPG-based sensing device and the tissue of the distal phalanx on the robustness of PWV determination and attempts to determine a contact force for which PWV determination is deemed most robust, according to the characteristics of PWV determination quality inferred from Figure 2.

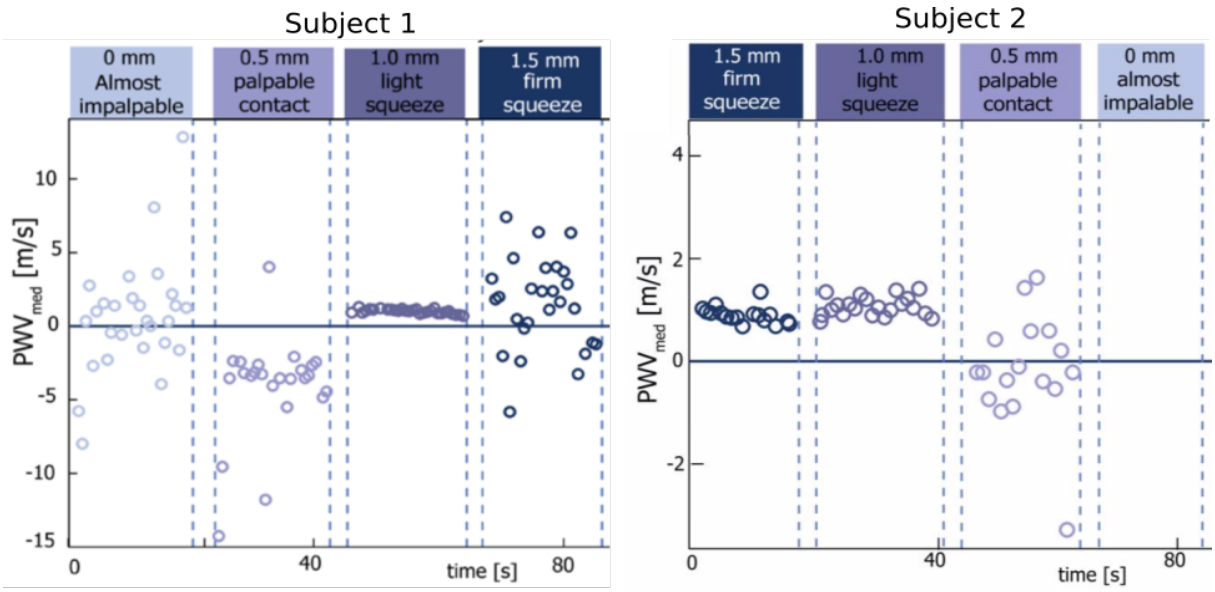

Figure 2 - Excerpt from image 8.7 by van Velzen, showing a dependency of PWV determination robustness on indentation depth with the tissue, which differs for two subjects [1]. PWV med is the value for the median of the six PWVs determined over six intervals.

Three characteristics for 'bad' PWV determination can be inferred from the work by van Velzen, and can be seen in Figure 2 [1]: 1. The signal is not detected at all, or completely filtered out due to bad quality, leaving no calculated PWV values (Subject 2, 0mm indentation); 2. The signal is highly variant (Subject 1, 1.5mm indentation); 3 The calculated PWV is a highly unrealistic and/or negative value (Subject 1 and 2, 0.5mm indentation). Further theoretical background in current techniques, PPG, and the MPA is provided in Appendix A.

Materials

The FA-MPA

The nature of the study, combined with preferences for sensor modularity required a redesign of the MPA as developed by van Velzen [1]. A statement of requirements (SOR) was composed according to which the Force-Alterable Multiphotodiode Array (FA-MPA) was designed and constructed (Figure 3). The full SOR is provided in Appendix B. The FA-MPA is a PPG-based sensor, providing alterable and determinable contact force for accurate and safe determination of the PWV in the vasculature of the distal phalanges of multiple test subjects. The sensor was finalized after a lengthy design process, the aspects and stages of which are elaborated on in Appendix C. For ease, the FA-MPA is presented in two parts: the sensor and the linear stage.

The sensor

The newly constructed sensor is shown in Figure 4, it comprises four SI-PIN photodiodes (850nm peak sensitivity) (SFH 2400, OSRAM Opto semiconductors GmbH, Regensburg, Germany) that are placed under a 90-degree angle of two Infrared LEDs (850nm peak intensity) (HT-170IRPJ, Harvatek, Hsinchu City, Taiwan) and one hyper red LED (645nm peak intensity) (LH R974, Osram Opto semiconductors). All LEDs and PDs that were used were surface mounted devices (SMD), meaning that they are attached to a flat surface of an underlying structure rather than plugged in**.** The Hyper red LED serves no true purpose in the current experimental protocol but was incorporated to anticipate the future final electrical and structural setup of the device to ensure any future discrepancies in light emission were attenuated. In the future, the hyper red LED might serve function in determination of blood oxygenation. All LEDs and PDs were soldered on 1x2 mm sections of print board and completed with two connecting pins to create a singular LED- or PD-module. A photograph of a PD-module is also shown in Figure 4. Modules were inserted into two separate female header arrays (MK 220 SMD, Fischer Elektronik, Lüdenscheid, Germany), creating one PD array and one LED array. The arrays were then secured in a custom made casing, designed with Solidworks 2016 (Dassault Systems, Tennessee, United States), which was 3D printed using black Polylactic Acid (PLA) in an Ultimaker Extended 2+ 3D printer (Ultimaker, Geldermalsen, Netherlands).

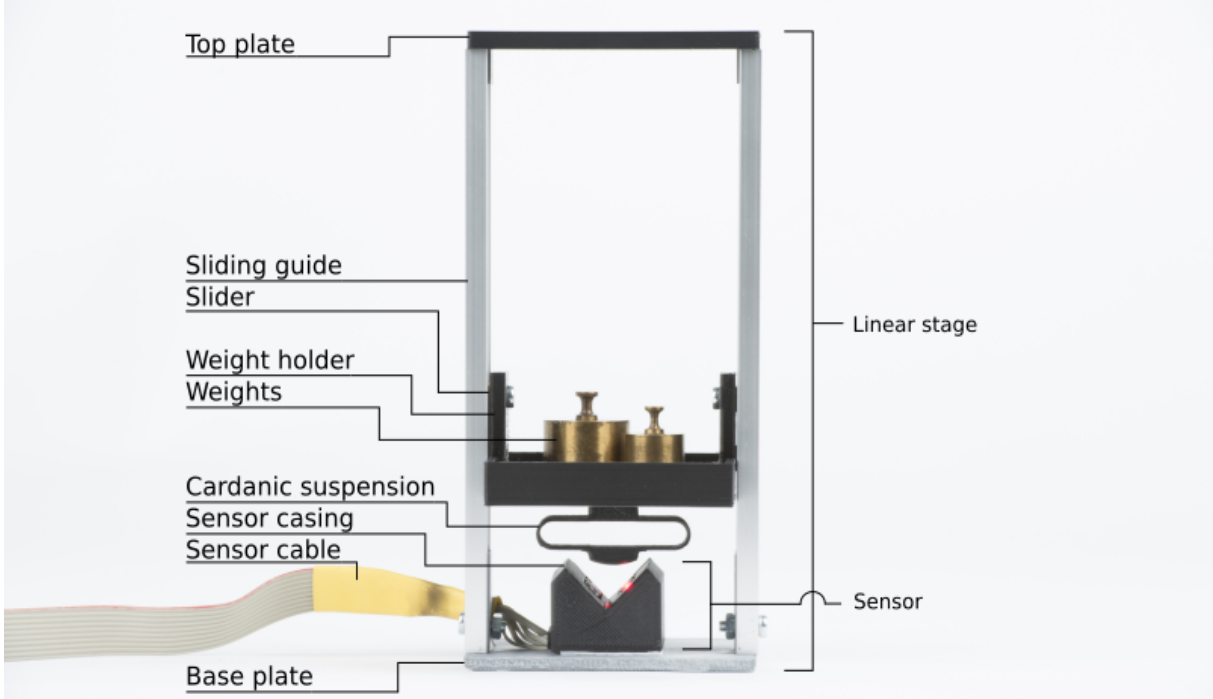

Figure 3 - Photograph of the front view of the FA-MPA. The weight holder contains two of the weights that were used during experimentation.

The electrical contacts were covered using clear tape, to prevent contact between the skin of the subjects and the electrical contacts and to prevent dirt from accumulating in the PD and LED arrays. Technical drawings of the sensor casing are provided in Appendix D. The female header arrays were then attached to external wiring, of which the electrical schematic is also provided in Appendix D. From the PD and LED arrays, a 10-p flatcable (TRU components, Conrad, Hirschau, Germany) runs to a 10-p female header connector (TE connectivity, Schaffhausen, Switzerland), completing the sensor. The sensor cable is fabricated out of a 10-p male header connector (TE connectivity), a generic 10-p shielded cable and a 25 pin D-connector (unknown manufacturer).

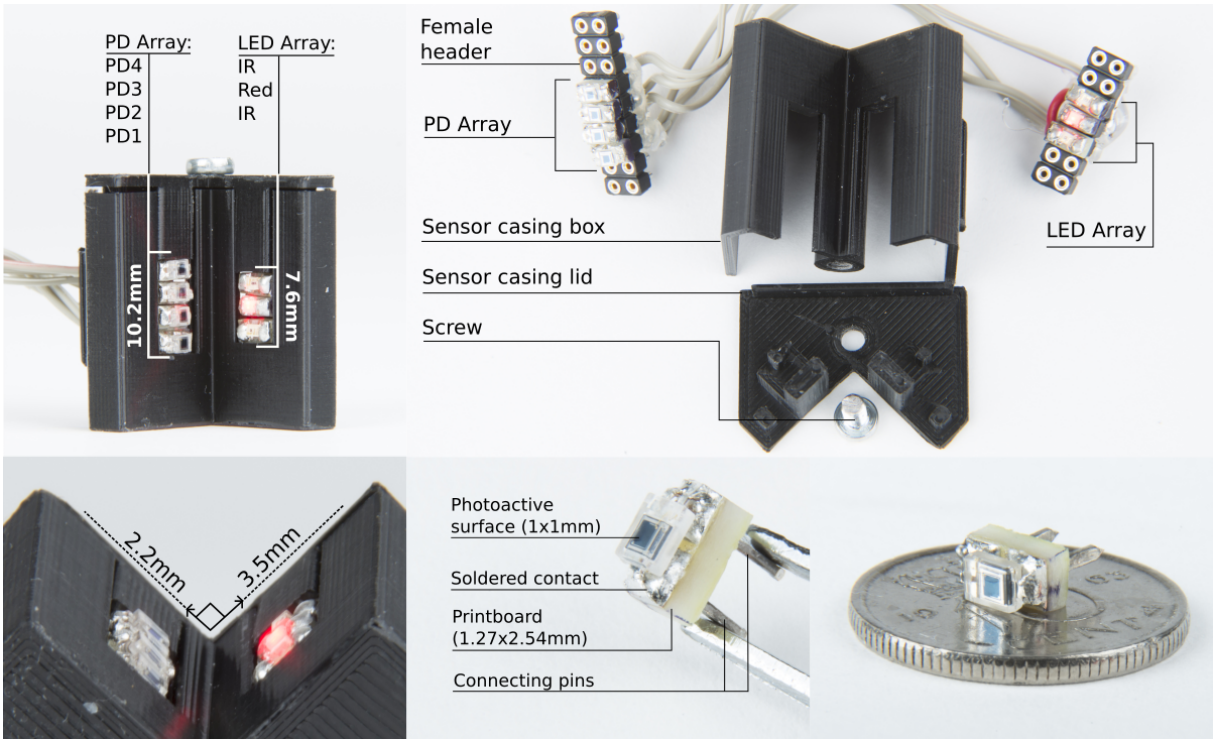

Figure 4 - Photographs of the experimental sensor and it's components. Top left: Top view of the experimental sensor. IR is infrared. Top right: Exploded view of the sensor internals. Bottom left: Close up of sensor top surface. Bottom middle: One PD module, held by tweezers. Bottom right: Size comparison between a PD module and a 10ct. coin.

The linear stage

The linear stage is shown in Figure 3 is the part of the FA-MPA responsible for adding increments of weight onto the distal phalanx, as to increase the contact force between the distal phalanx and the sensor and moreover to apply this force in a manner that is to minimize non-perpendicular components. The linear stage consists of two aluminum linear sliding guides (Drylin N-series, IGUS, Soesterberg, Netherlands) that are placed vertically onto a base plate. The top of the guides was then closed with a top plate. To the sliders that move in the linear guides, a small plastic container is attached that can hold differing weights. Under the basket a monolithic elastic cardanic suspension is attached to mitigate possible askew or point load on the finger other than right over the distal phalanx. All components except the sliders and weights were printed using black PLA in the same Ultimaker Extended 2+ as was used for the sensor casing. Technical drawings of the printed stage components are provided in Appendix B. To complete the device, the sensor is secured in the center of the base plate right underneath the cardanic suspension.

Experimental setup

The sensor and linear stage were secured to the top plate of a digital scale (Kern EMB 1200-1, Kern & Sohn, Balingen, Germany) to prevent the FA-MPA from moving around and to be able to determine the force between the distal phalanx and the sensor during experimentation, which could be directly calculated from the weight the scale indicated. For data acquisition and processing, an NI-USB 6211 Multifuction Data Acquisition system (National Instruments, Austin, TX, USA) and LabVIEW 2010 software (National Instruments, Austin, TX, USA) were used. The data acquisition system converted the four analog PPG signals from the FA-MPA to digital components with a sampling frequency of 250kHz. At this sampling frequency of 62.5kHz per photodiode, the maximum speed that could be ‘seen’ with a photosensitive surface with a width of 1mm is 62.5 m/s, which is well above the expected PWVs that are to be measured [12]. A stopwatch (Built in Application, Iphone 6, iOS 12.1.2, Apple Inc., Cupertino, Californië, United States) was used to time intervals for data acquisition. A photo of the experimental setup is shown in Figure 5. Furthermore, a digital caliper was used for measurements on the distal index phalanges of each subject. A Datascope Radical RDS1 (Masimo, Irvine, California, United States) was used for heart rate measurements. Lastly, a Datex Ohmeda S5 (GE healthcare, Chicago, Illinois, United States) modular unit’s automatic sphygmomanometer function was used for blood pressure measurements. A schematical top view of the experimental setup is also shown in Figure 5.

Methods

Study population

From earlier measurements performed with the MPA, it was found that the PWV in the peripheral vasculature of the distal phalanx of healthy subjects was 0.9±0.6 m/s (mean ± SD) [1]. Using this effect size with a two tailed 5% significance level and 90% power in a sample size power analysis opted that significant results could be achieved when using 7 subjects. This number was expanded to 9 to ensure possible later exclusions could be mitigated, and subsequently tripled to leave the possibility for clustering the subjects in three cohorts, judging on subject specific parameters such as phalanx volume or length. Thus, the total number of subjects that was recruited was 27. Healthy male and female subjects between 18 and 35 years of age and with a present distal phalanx on the left index finger were included in this experiment. Subjects were excluded if they had any known cardiovascular affects, used any incompatible medicine, or suffered from one of the following: Peripheral vascular disease; Diabetes; Tremor; Muscle or skeletal injuries in the upper limb; Hematopoietic disease. This study was approved by the Human Research Ethics Committee of the Delft University of Technology in the Netherlands.

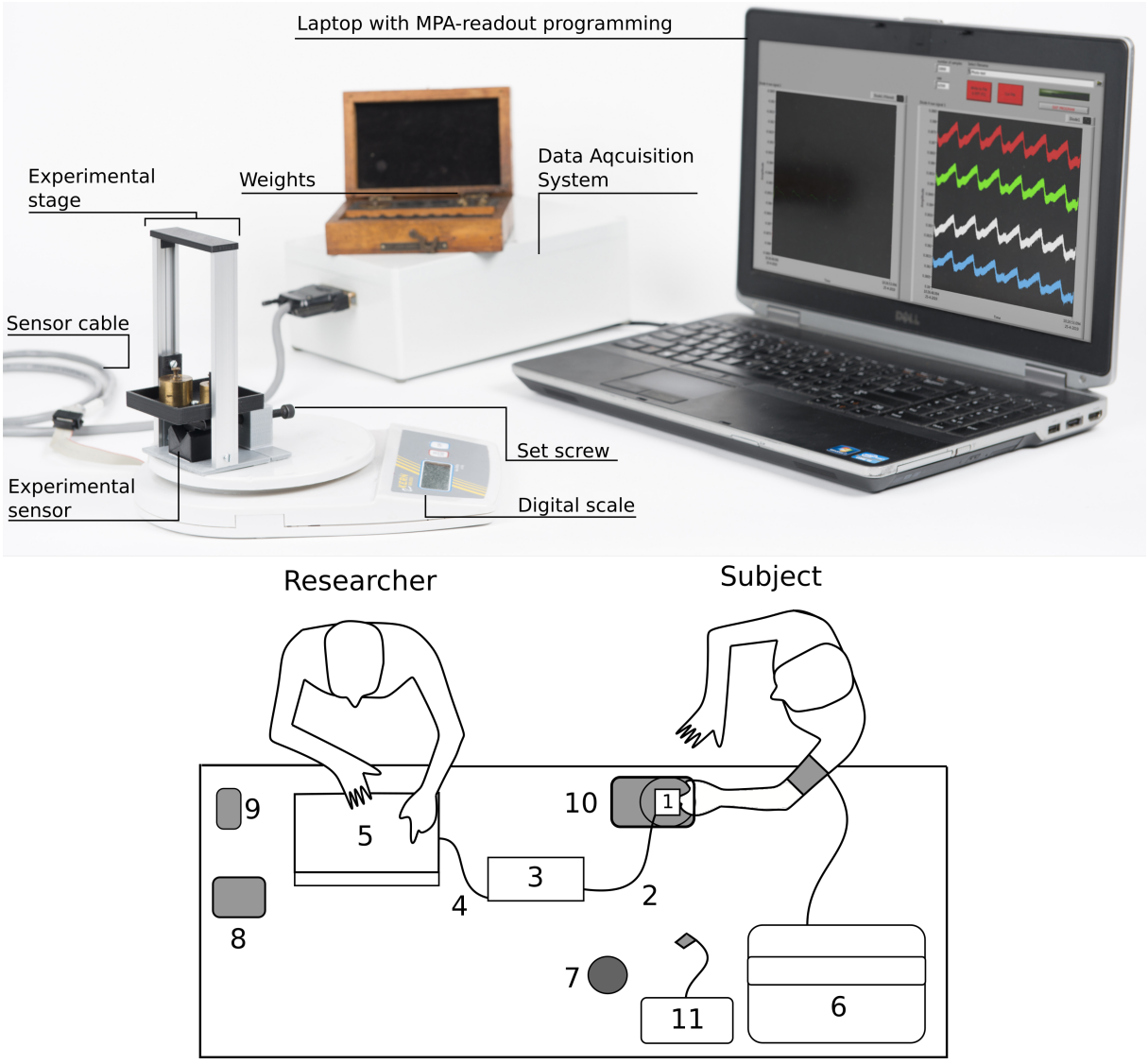

Figure 5 - Top: Photograph of the components of the experimental setup. Not shown in this image: Datascope Radical, Datex Ohmeda, Stopwatch, Caliper, Thermometer. Bottom: Seating arrangement and layout of experimental setup, where: 1 – FA-MPA; 2 - Sensor cable; 3 - DAC-unit; 4 - USB-B data cable; 5 – Laptop; 6 – Blood pressure sensor; 7 – Weights; 8 – Thermometer; 9 – Stopwatch; 10 – Digital scale; 11 – Heart rate sensor.

Measurement protocol
Prior to information gathering and measurements, informed consent was obtained from each subject. After this, subject specific characteristics such as age, biological sex, body height, body weight, distal index phalanx dimensions, blood pressure and heart rate at rest was gathered. Furthermore, information about substance (ab-) use, use of medication and known physical affects was gathered from the subject. Phalanx width and height were measured parallel and perpendicular to the nail bed and at 15% of the length of the phalanx, measured from the Digital Inter-Phalangeal Joint Crease (DIPJC), shown schematically in Figure 6. Distal phalange geometry for volume calculation was assumed to be a combination of an elliptic cylinder and a half ellipsoid. Information was collected on the case-report form, which was filled out for each experiment (Appendix E).

All measurements were conducted under standardized, stable conditions in a quiet, temperature controlled room by the author. The subject was sitting upright on a chair, with their entire lower left arm lying at heart level on a table. Their left index finger was placed in the experimental setup, with their distal index phalanx on the sensor. The screw was adjusted such that it constrained the subject from placing their distal phalanx too far on the sensor and such that the edge of the first photodiode exactly lined up with the DIPJC (Figure 6). The screw remained in the same position for all measurements with the same subject, to provided tactical and visual feedback for the correct placement of the index phalanx on the sensor. The hand and experimental stage were then elevated with respect to one another if necessary to ensure the index finger was horizontal during the experiment. The subject was asked to remain still during the duration of the measurement and not speak or move unless instructed to, or if they would like to discontinue the experiment.

The experiment consisted of 7 individual measurements per subject. Measurement 1 was performed without added weight and without the weight holder in the setup. For each measurement after this, the weight holder was placed in the setup and weight was placed in the weight holder, which was then lowered until the cardanic suspension rested on top of the distal phalanx. The added weight ranged from 0 to 300g (0-2.94N) with 50g (0.49N) increments, taking into account the weight of the weight holder itself (20g, 0.2N) (Eq. (4)). First, a measurement without added weight was performed (measurement 1). The order of the following measurements was randomized beforehand with the ‘randperm(6)’ functionality of MATLAB R2018a (Mathworks, Natick, Massachusetts, United States). The randomized measurement orders per subject are provided in Appendix E. Each measurement had a duration of 2 minutes, which was timed with a stopwatch. After each measurement, the subject was asked to remove their distal phalanx from the sensor and move it around momentarily to prevent possible loss of circulation due to the muscles remaining static for too long. The seating arrangement and experimental layout is shown schematically in Figure 5.

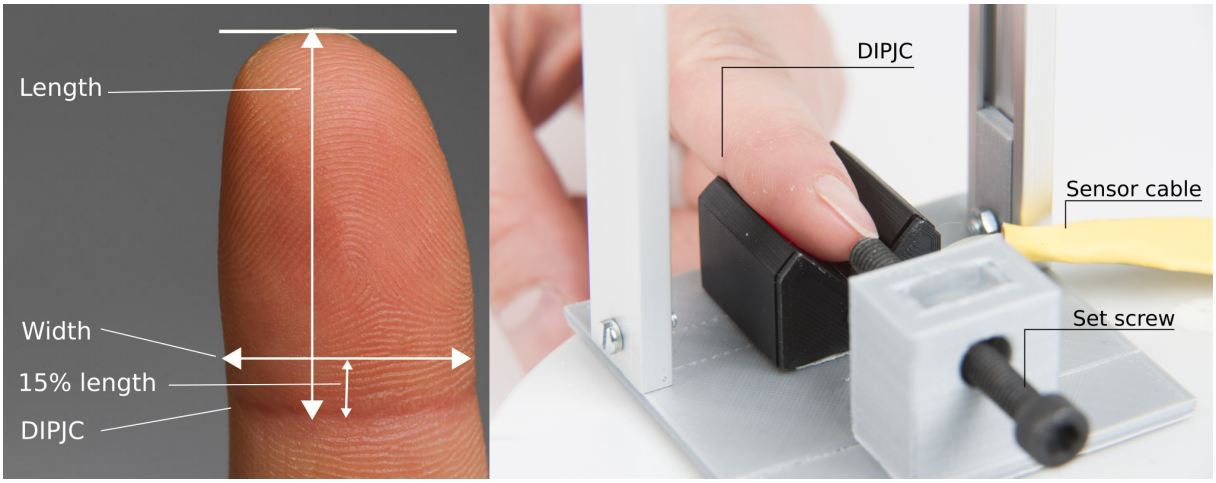

Figure 6 - Left: Schematic for the DIPJC measurements (Image courtesy of Fineart America). DIPJC = Distal interphalangeal joint crease. Right: Photograph of the placement of the distal phalanx on the sensor.

Data processing and PWV analysis

Raw PPG-signal was collected from each photodiode individually during each measurement at a sampling frequency of 62.5 kHz (Figure 7A). This raw signal was then filtered for high frequency noise by a fourth order low-pass Butterworth filter with a cutoff frequency of 9 Hz and the signal was normalized by removing the trend with a Butterworth filter with a cutoff frequency of 0.05 Hz to reduce environmental factors such as change in ambient light in the room and account for the offset between the four PPG signals due to differences in series resistance of the individual photodiodes. From the PPG signal of photodiode 1, the peaks of the PPG signal were detected using the MATLAB 'R-Peakdet' function, each coinciding with minimum expansion of the PPDA just before one heartbeat (Figure 7B) [13]. The times between these peaks were averaged for the entire measurement, yielding an average 'Systolic Interval'. The PPG signal was then inverted, showing the expansion of the PPDA (Figure 7C), and all four signals were simultaneously clipped ¼ Systolic Interval before and ½ Systolic Interval after peak of the PPG signal, leaving one waveform for each photodiode per systole (Figure 7D).

The individual waveforms were tested according to the 7-step-PWV-filter designed by van Velzen to see if the waveform had the known characteristics of a proper PW [14]. From this filter process, the Pulse Wave Quality Ratio (PWQR) was determined as the ratio between suitable PWs (PWs with a proper waveform) and unsuitable PWs during a measurement, resulting in a value between -1 and 1, indicating the average quality of the detected PWs [1]. This relation is shown in Eq. (2), where S is the number of suitable PWs, U is the number of unsuitable PWs and the correction percentage is the percentage of waveforms that was filtered out by the 7-Step-PW-Filter.

$$PWQR = \frac{S-U}{S+U} = 1 - 2 * (Correction\ Percentage/100) \quad \text{Eq. (2)}$$

From each of the four waves, the maximum of the second derivative of the PW was determined as the foot of the PW, indicating the onset of the PW. The temporal difference between the occurrence of these onsets at the four PDs was then determined and used to calculate the PWV between the photodiodes in six different combinations (1-2, 2-3, 3-4, 1-3, 2-4 and 1-4) (Figure 4) to increase calculation robustness. Outliers of these six values were removed using a Hampel identifier, stating that a PWV value should be 3 times the standard deviation larger than the local median. The median of the remaining PWV values was then used as final PWV value for that wave (Figure 7E). This value will be referred to as 'the median PWV'. Of these median PWV values, the 'Mean Median PWV' and 'PWV variance' are determined to assist in further analysis.

Polynomial fit order was determined by the minimum fit variance, which is calculated using Eq. (3) [15]. Where: Sr is the sum of the residuals for the m^{th} order polynomial; n is the number of data points and m is the order of the polynomial. The value for m for which the fit variance had a minimum or after which it did not decrease further was chosen as the order of the polynomial fit.

$$Fit\ variance = Sr(m)/(n-m-1) \quad \text{Eq. (3)}$$

Values for the weight that was measured during the measurement was converted to contact force using Eq. (4) where $F_{contact}$ is the contact force between the distal phalanx and the sensor in Newton, weight measured is in grams and g = 9.81m/s^2.

$$F_{contact} = weight\ measured * 10^{-3} * g\ [N] \quad \text{Eq. (4)}$$

Statistical analysis

Results for the PWQR, the PWV variance and the Mean Median PWV were ordered into 8 'weight groups', ranging from 0 to 400g with 50g increments, according to the weight that was measured on the digital scale during that measurement. One sided analysis of variance (ANOVA) was performed on the values for the PWV variance and the Mean Median PWV to determine if there was a statistical difference between the weight groups. The ANOVAs were performed with StatPlus:mac LE (AnalystSoft, Walnut, California, United States). Also, correlation between PWV Variance and measured weight and subject specific parameters such as BMI and Phalanx volume, length, height and width were investigated using the linear regression tool of MATLAB R2018a.

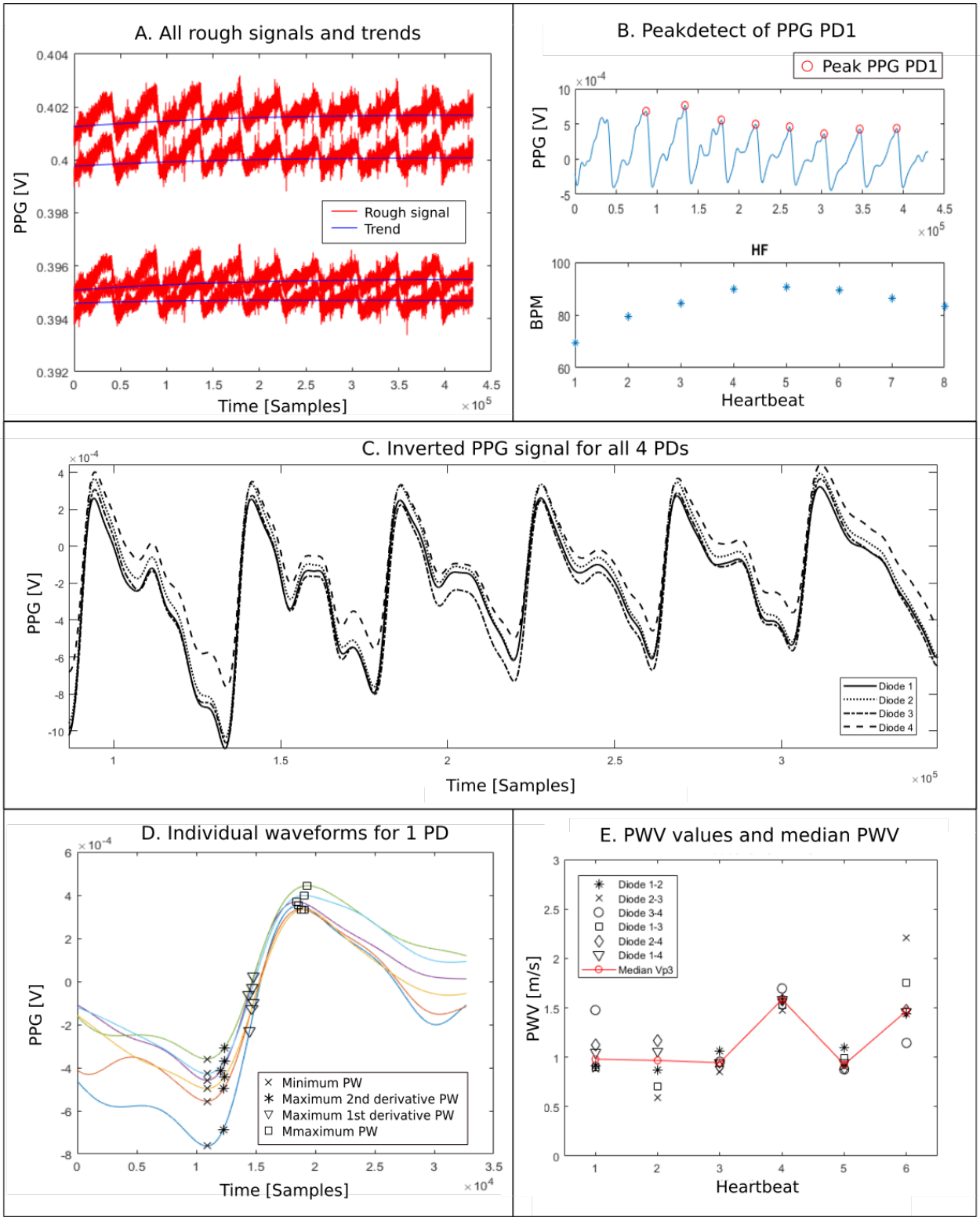

Figure 7 - Order of data processing steps of one test measurement with: A. Rough signals and trends for 4 PDs where PPG = Photoplethysmography; B. Detected peaks on PPG signal for PD1; C. Inverted PPG-signals for all PDs, showing the PWs; D. Individual clipped waveforms for one photodiode, with markers on locations for Minimum, Maximum of 2nd Derivative, maximum of 1st derivative and Maximum; E. Calculated PWV values for all PD combinations and the median PWV per heartbeat.

Results

27 subjects were included in this study (16 male, 11 female), resulting in 27 datasets containing 7 measurements each. Demographic characteristics of the study population are shown in Table 1. PWVs calculated over PD combinations containing PD 1 were excluded, since these showed systematic inaccuracies that could be traced back to sensor positioning according to van Velzen [1]. Data from all 7 measurements from 1 male subject was excluded because the experiment protocol was not followed correctly during these measurements.

Table 1 – Demographic characteristics of the study population. * = No. (%). ** = mean ± SD

	n = 27
Biological sex* (male)	16 (59)
Age** [Years]	26 ± 2
Height** [cm]	179 ± 10
Weight** [kg]	76 ± 13
Body mass index** [kg/m^2]	23.5 ± 2.9
Smoker* (yes)	3 (11)
Resting heart rate** [bpm]	72 ± 11
Systolic blood pressure** [mmHg]	129 ± 12
Diastolic blood pressure** [mmHg]	75 ± 11
Mean arterial pressure** [mmHg]	94 ± 12
Distal phalange volume** [cm^3]	4.3 ± 1.0

For the individual measurements, the Pulse Wave Quality Ratio (PWQR) was determined. 43 measurements were excluded for further analysis because the PWQR of these measurements was lower than 0. PWQR values per measurement are shown in Figure 8, together with a 3rd degree polynomial fit to the data. A total of 139 measurements were left for further analysis. Measurements were ordered according to the weight that was measured on the digital scale during that measurement and combined into weight groups ranging from 0g to 400g with 50g increments. The values for PWQR, the Mean Median PWV and PWV variance were calculated and subsequently averaged over all measurements per weight group. These results are shown in Table 2. PWV Variance values per measurement are shown in Figure 9. A boxplot for Mean Median PWV values per weight group is shown in Figure 10.

A one-way analysis of variance (ANOVA) was performed on the values for the Mean Median PWV and the PWV variance for each of the 8 weight groups, the results of which are shown in Table 3 and 4, respectively. The reason for the low values of the mean and sum of the Mean Median PWV for the 50-100g weight group in Table 2 is the presence of a higher fraction of negative Mean Median PWV values in this group and a stronger influence of these values on the mean, as can be seen in Figure 10.

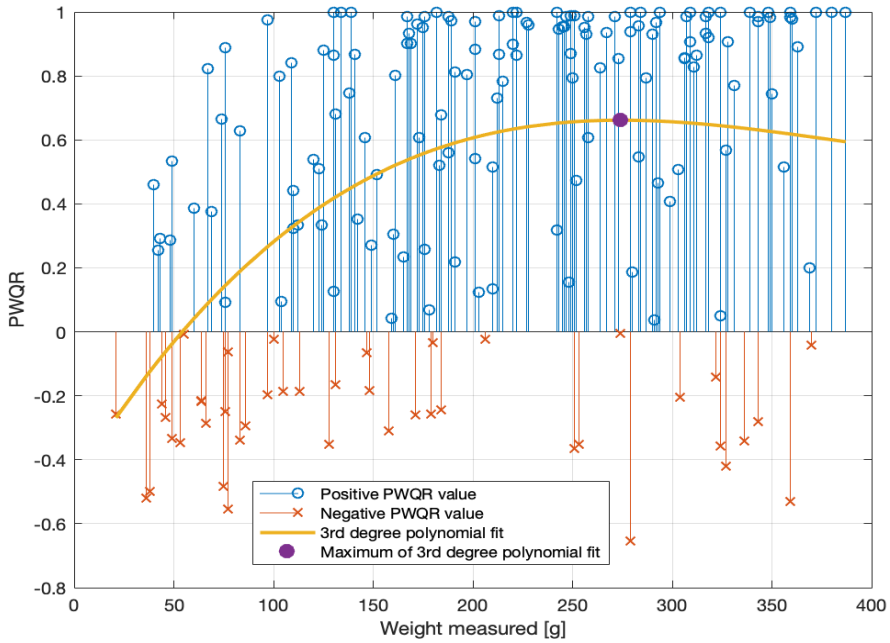

Figure 8 – Stem plot for PWQR values per individual measurements, before exclusion, and 3rd degree polynomial fit to all PWQR values.

Table 2 – Descriptive statistical values for PWQR, Mean Median PWV and PWV Variance, determined per weight group. Values are absolute or in Mean ± SD. PWV No. of excl. is the total number of excluded measurements in that group where PWQR < 0. Sample size is no of measurements after exclusion.

Descriptive Statistics of PWQR, Mean Median PWV and PWV Variance

	PWQR					Mean Median PWV				PWV Variance			
Groups	*Sample size*	*Sum*	*Mean*	*Variance*	No. of Excl.	*Sample size*	*Sum*	*Mean*	*Variance*	*Sample size*	*Sum*	*Mean*	*Variance*
0-50g	11	-0.28	-0.3	0.15	6	5	1.48	0.30	0.51	5	23.02	4.60	30.73
50-100g	20	1.57	0.08	0.24	12	8	0.07	0.01	0.97	8	40.36	5.05	15.27
100-150g	28	11.44	0.41	0.18	7	21	13.75	0.66	1.55	21	152.52	7.26	29.88
150-200g	29	14.88	0.51	0.20	5	24	22.26	0.93	2.05	24	119.65	4.99	23.03
200-250g	26	19.39	0.75	0.11	1	25	20.93	0.84	2.45	25	165.27	6.61	81.45
250-300g	28	17.21	0.61	0.23	4	24	15.47	0.65	3.38	24	173.02	7.21	117.27
300-350g	29	17.10	0.59	0.28	7	22	26.15	1.19	1.48	22	109.75	4.99	80.65
350-400g	11	7.88	0.71	0.23	1	10	10.99	1.10	1.75	10	48.84	4.88	100.87
Total	182	182	0.49	0.25	33	139		0.80	2.05	139		5.88	63.42

Table 3 - Results for one-way Analysis Of Variance (ANOVA) for the PWQR ordered by weight group. DF = Degrees of freedom; SS = Sum of squares; MS = Mean squares;

ANOVA of PWQR

Source of Variation	***DF***	***SS***	***MS***	***F-ratio***	***p-value***	***F crit***	***Omega²***
Between Groups	7	9.45	1.35	6.57	6.91E-7	2.06	0.18
Within Groups	173	35.79	0.21				
Total	180	44.96					
Residual standard error		0.45					
Hartley Fmax *(DF = 8, 28)*		2.50					
Cochran C *(DF = 8, 28)*		0.17					
Bartlett Chi-square *(DF = 7)*		6.33	***p-value***	0.50			

Table 4 - Results for one-way Analysis Of Variance (ANOVA) for the Mean Median PWV, ordered by weight group. DF = Degrees of freedom; SS = Sum of squares; MS = Mean squares;

ANOVA of Mean Median PWV

Source of Variation	***DF***	***SS***	***MS***	***F-ratio***	***p-value***	***F crit.***	***Omega²***
Between Groups	7	11.94	1.70	0.83	0.57	2.08	-0.01
Within Groups	131	270.42	2.06				
Total	138	282.36					
Residual standard error		1.44					
Hartley Fmax *(DF = 8, 24)*		6.63					
Cochran C *(DF = 8, 24)*		0.24					
Bartlett Chi-square *(DF = 7)*		9.41	***p-value***	0.23			

Table 5 - Results for one-way Analysis Of Variance (ANOVA) for the PWV Variance, ordered by weight group. DF = Degrees of freedom; SS = Sum of squares; MS = Mean squares;

ANOVA of PWV Variance

Source of Variation	***DF***	***SS***	***MS***	***F-ratio***	***p-value***	***F crit***	***Omega²***
Between Groups	7	155.03	22.14	0.34	0.94	2.08	-0.03
Within Groups	131	8,606.70	65.70				
Total	138	8,761.72					
Residual standard error		8.11					
Hartley Fmax *(DF = 8, 24)*		7.68					
Cochran C *(DF = 8, 24)*		0.24					
Bartlett Chi-square *(DF = 7)*		25.46	***p-value***	5.80E-4			

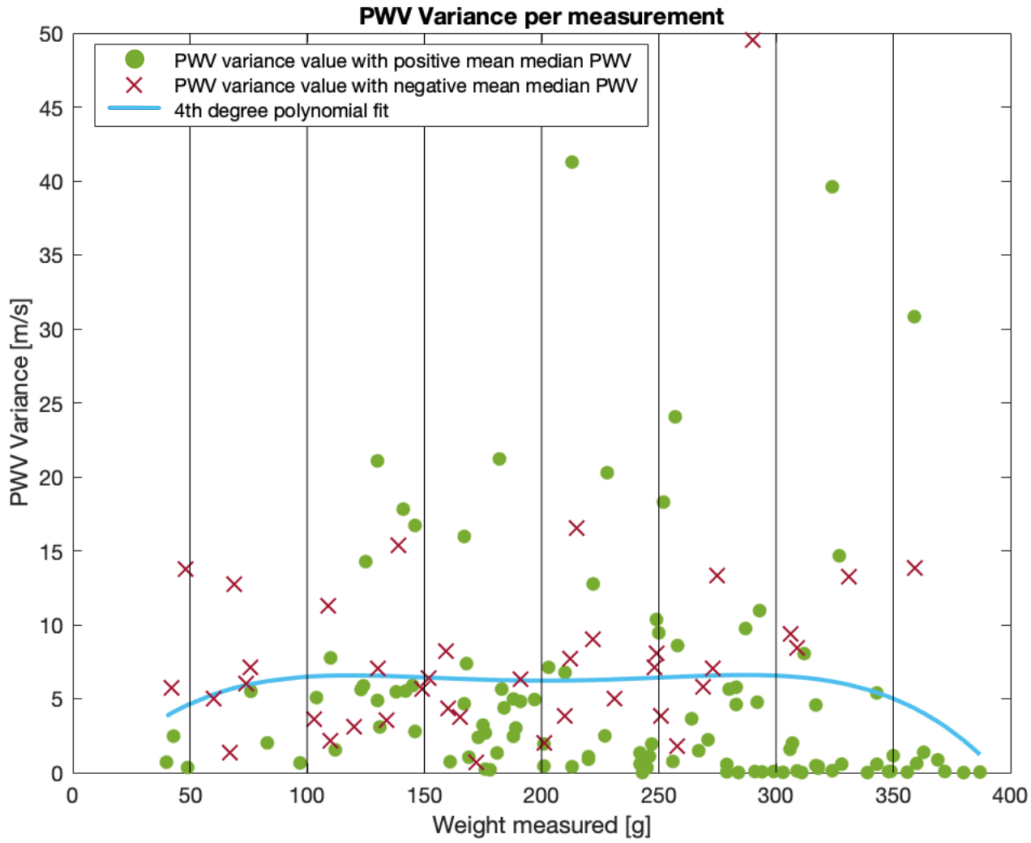

Figure 9 - Variance values for individual measurements, showing for which measurement the Mean Median PWV was negative. The 4th order polynomial fit was calculated for all variance points, both with negative and positive values for mean median PWV.

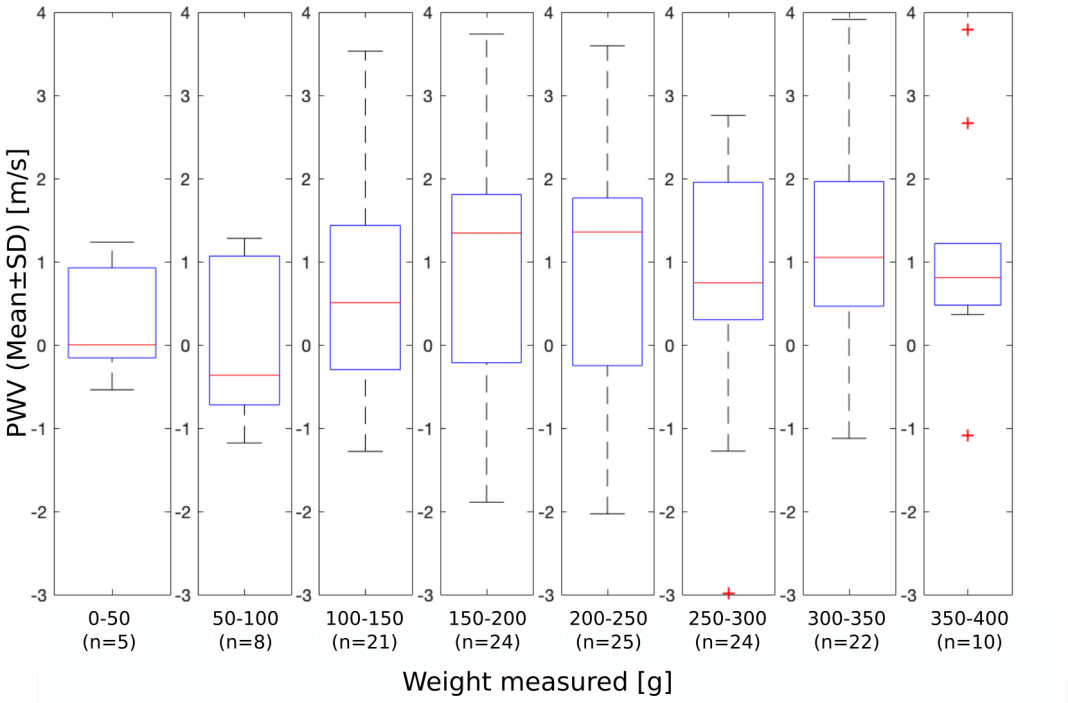

Figure 10 - Boxplot for the Mean Median PWV values, averaged per weight group. n = Number of included measurements for that weight group.

Discussion

Results

This study aimed to find a contact force that ensured optimal signal robustness for the determination of the PWV in the peripheral vasculature of the distal phalanx, using a novel PPG-based multi-purpose sensing device. For PWV calculations to be deemed robust, they were tested on three desirable characteristics: 1 – Proper wave shapes, meaning a high PWQR; 2 – Low PWV variance. 3 – Realistic (non negative) values for Mean Median PWV in the PPDA of around 0.8 m/s [16].

Indications of robustness dependency on contact force were abundant, as found by van Velzen [1]. Systematic occurrence of negative median PWV values, sudden shifts between negative and positive median PWV values and large differences in variance were all seen both intra- and inter-measurement and even between different diode combinations. A good example from the rough measurement data is shown in Figure 11, which shows the PWV values calculated from data gathered with subject 21 during measurement 3. Although the PWQR was high (PWQR = 0.99), variance was still high (41.2) and the PWVs that were calculated were abnormally high (max 30.15 m/s), so the contact force during this measurement ultimately was non-optimal. Between heartbeats 65 and 90, it can be seen that values of PWV calculated between PD 3 and 4 suddenly shift to negative with seemingly low variance, which might indicate a movement of the distal phalanx by the test subject, causing a positioning artifact or a momentarily in- or decrease of contact force between the distal phalanx and the sensor. This indicates that the test protocol was not sufficiently effective in eliminating movement artifacts.

Visually, results between measurements showed improvement upon the adding of weight and increasing the contact force between the distal phalanx and the sensor. However, ANOVA only resulted in a significant effect between weight groups for the PWQR, thus necessity arose for further qualitative judging of the data. Primary analysis by the 7-Step-PW-filter allowed calculation of PWQR per measurement. This showed that the trend for the PWQR (3rd degree polynomial, variance of the data to the polynomial fit (Fit variance) = 0.27) quickly rises and then drops slowly for a measured weight of 200g and higher (Figure 8) and with a highest average for the 200-250 group (PWQR = 0.75**Fout! Verwijzingsbron niet gevonden.**) according to Table 2. Secondly, low PWV variance was preferred. In the range of measured weight of 200-400g, the highest weight group showed the lowest mean variance according to Table 2. Figure 9 shows that the 4th degree polynomial fit to the variance data is visually horizontal and the fit variance was high (64.69). Since Figure 10 clearly shows a cluster of very low PWV variance values for higher weight groups (250-400g) it was believed the fit was strongly influenced by outliers of PWV variance, even though strong median PWV outliers were eliminated with a Hampel filter during pre-processing of the data. Lastly, Mean Median PWV values found for measurements in the highest weight group (350-400g) visually showed the best comparison with PWV in the peripheral vasculature that was found in other studies of around 0.8 m/s [1, 16].

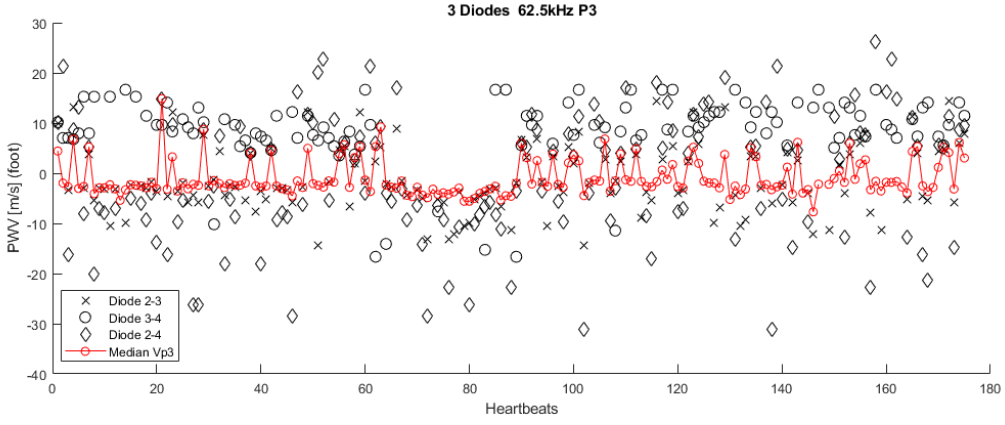

Figure 11 - PWV calculations in subject 21, measurement 3 (100g added weight, 213g measured weight (2.09N contact force).

By qualitatively judging the data on the three robustness characteristics of high PWQR, low PWV variance and reality of Mean Median PWV, an advice can be given on a contact force between 2.45 and 3.92 N, according to Eq. (4). Preferably, a large cohort study is performed in the future to investigate the PWV determination robustness within this contact force range, to further investigate the influence of subject specific parameters but also seeking out an upper limit of contact force (above 3.9N) for which the PW can still be detected by the FA-MPA since this is not yet visible in the study data. To substantiate and illustrate, a test measurement of 30 seconds was performed on the distal index phalanx of the author (healthy male of 26 years old with a BMI of 22.6), with a measured weight of 452g. Visual qualification of the measurement data showed that wave shapes were either nearly non-visible or heavily distorted. After manual sensitization of the 'RPeakdetect' function, PWQR for this measurement was -0.62, substantiating the theory that there is an upper boundary for PWV determination robustness that has not been found during this study [13].

Finally, an indication of dependency on subject specific parameters arose from large differences in PWQR values between different subjects. For example, all measurements preformed on subject 16 resulted in a negative PWQR, all measurements for this subject averaging at -0.26, whereas all measurements performed on subject 21 resulted in a positive PWQR, all measurements for this subject averaging at 0.99. Since the differences in average PWQR were so large between these subjects, regardless of the measured weight, the PWV variance was tested for correlation with subject specific parameters. A linear regression fit to the data showed no significant correlation between the PWV variance and the weight measured, and the subject BMI ($p = 0.16$), phalanx volume ($p = 0.83$), phalanx length ($p = 0.65$), phalanx height ($p = 0.86$) or phalanx width ($p = 0.96$).

Study limitations

After the choice was made to abandon the 'portable' experimental sensor (discussed in Appendix C) a considerable amount of sensor characteristics were adapted to the new static experimental setup, two of the most influential being sensor casing size and geometry and modularity of electrical sensor components. PD modules being able to move around in the casing and being too tightly fit into the sensor casing is believed to have deteriorated the quality of the sensor in terms of structural integrity and quality of electrical infrastructure.

This deterioration was possibly increased by the lack of fabrication techniques at hand during construction of the experimental sensor. The PD and LED modules were handmade by the author, using a conventional soldering iron, whereas surface mounted components, as were used in the FA-MPA, are most often secured using solder reflow techniques to ensure fabrication quality [17]. Because of this lower quality, placement of the PDs and LEDs on the printboard was also not always flush with the edges or parallel to the surface of the printboard, possibly introducing measurement artifacts. The same lack of electrical integrity can be stated for the connection between the female headers and the sensor cable cores. This connection was soldered and then secured using a hot melt adhesive, but after the experiments it was found that the solder came loose after prolonged handling. No defects were detected during experimentation, but functioning of the sensor was found to be sub-optimal afterwards.

Lastly, although not hazardous for the subject or experimenter, the soldered contacts of the PD and LED modules laid bare. In early experiments, this caused the noise on individual PPG signals to be amplified greatly. Although noise was present, the low-pass Butterworth filter at 9Hz proved efficient, leaving enough proper wave shapes according to the 7-step-PWV-filter for the PWQR to be positive for most of these measurements. The measurements for which this was not true were measurements with low measured weight, so it is expected the low PWQR is due to the low contact force and not the present noise in the signal. The occurrence of higher signal noise was mitigated by placing clear tape over the soldered contacts of the modules, however it does signal a lack of technical integrity which needs to be addressed, because the need for higher intensity filtering of the noise can affect the higher frequency components of the desired signal, effectively deteriorating the accuracy of the determination of the exact location of the second derivative of the PW waveform. Therefore it is highly recommended to redesign the FA-MPA as a purely experimental sensor, disregarding earlier notions of maximum size or weight, and then rebuilding the sensor focusing solely on structural and electrical integrity to benefit signal robustness. A more detailed recommendation on sensor redesign and rebuild is provided in Appendix F.

Besides technical limitations it is believed that the measurement protocol did not properly mitigate placement and contact force discrepancies. According to van Velzen, the orientation at which the distal phalanx was placed on the sensor (rotation and translation of distal phalanx with respect to the PD and LED array) was optimal. However, changes in robustness of PWV determination were found that could not directly be explained by the alteration of contact force. An example is the sudden intra-measurement changes between positive and negative values for the median PWV as can be seen in Figure 11. This leads to believe the protocol did mitigate the possibility that positioning of the distal phalanx on the sensor was not performed properly by the subjects, nor did it ensure that this was checked sufficiently by the experimenter. Still finding placement and movement artifacts with a measurement protocol that should mitigate these poses the question if a sensor based on the MPA is a viable technique in clinical practice at all, if movement and placement artifacts are so difficult to eliminate. A more detailed recommendation on measurement protocol is provided in Appendix F.

Furthermore, the weight that was measured during the measurements sometimes fluctuated as much as 50g in a single measurement. A gradual change in measured weight was always observed downward, which leads to believe this was caused by relaxation of the muscles, causing less of the weight of the hand and arm to be resting on the sensor. For these occasions, the mean of the outermost (maximum and minimum) values that were observed was registered as the weight measured during the measurement. Furthermore, sudden changes in weight measured were observed during sudden movements of the subject. Sometimes this happened during coughing or sniffling, but often times there was no indication as to why the contact force suddenly peaked. The measurements during which these force discrepancies occurred were hand-checked for strong deviations in median PWV values and deemed eligible for inclusion. Nevertheless these occurrences are signs that the measurement technique for contact force can be greatly improved upon. Together with the advice to redesign the FA-MPA as a purely experimental sensor, it is strongly advised to redesign the linear stage (Shown in Figure 3) to incorporate a force sensor between the base plate and the sensor casing, to provide the ability to log real-time contact force data that can be directly coupled to calculated PWV values, providing a clearer and more accurate image as to how the actual contact force affects the PWV determination.

Conclusion

The results of this study showed that an optimal contact force range could not be numerically substantiated for all three characteristics the data was tested on. Only the PWQR showed significant difference between weight groups. A polynomial fit to the PWQR data showed a clear maximum between 200-400g (1.96-3.92N). However, with the sharp decrease of the PWQR during the test measurement at 452g it is recommended not to exceed 4.43N. Further strong recommendations for a force range for high robustness of PWV determination can be made on qualitative analysis of the experiment data. In the range of 200-400g, PWV variance showed the best values for the 350-400 weight group and Mean Median PWV values proved realistic for this weight group. Therefore it is recommended to use the force range of 1.96 to 4.43N as the basis for future development of a wearable PPG-based sensor for PWV determination in the vasculature of the distal phalanx and as the basis of measurement protocol formation in future experiments regarding PWV determination robustness on contact force.

References

1. van Velzen, M.H.N., *The Speed Of Waves - Measuring the velocity of pressure pulse waves traveling through blood in the peripheral blood vessels*. 2019, Erasmus Universiteit Rotterdam.
2. Roth, G.A., et al., *Global and regional patterns in cardiovascular mortality from 1990 to 2013.* Circulation, 2015. **132**(17): p. 1667-78.
3. Laurent, S., et al., *Aortic stiffness is an independent predictor of all-cause and cardiovascular mortality in hypertensive patients.* Hypertension, 2001. **37**(5): p. 1236-41.
4. Zieman, S.J., V. Melenovsky, and D.A. Kass, *Mechanisms, pathophysiology, and therapy of arterial stiffness.* Arterioscler Thromb Vasc Biol, 2005. **25**(5): p. 932-43.
5. Gosling, R.G. and M.M. Budge, *Terminology for describing the elastic behavior of arteries.* Hypertension, 2003. **41**(6): p. 1180-2.
6. Quinn, U., L.A. Tomlinson, and J.R. Cockcroft, *Arterial stiffness.* JRSM Cardiovasc Dis, 2012. **1**(6).
7. Cecelja, M. and P. Chowienczyk, *Role of arterial stiffness in cardiovascular disease.* JRSM Cardiovasc Dis, 2012. **1**(4).
8. Boutouyrie, P. and S.J. Vermeersch, *Determinants of pulse wave velocity in healthy people and in the presence of cardiovascular risk factors: 'establishing normal and reference values'.* Eur Heart J, 2010. **31**(19): p. 2338-50.
9. Hamilton, P.K., et al., *Arterial stiffness: clinical relevance, measurement and treatment.* Clin Sci (Lond), 2007. **113**(4): p. 157-70.
10. Willum-Hansen, T., et al., *Prognostic value of aortic pulse wave velocity as index of arterial stiffness in the general population.* Circulation, 2006. **113**(5): p. 664-70.
11. Allen, J., *Photoplethysmography and its application in clinical physiological measurement.* Physiol Meas, 2007. **28**(3): p. R1-39.
12. van Velzen, M.H.N., et al., *Design and Functional Testing of a Novel Blood Pulse Wave Velocity Sensor.* Journal of Medical Devices, 2017. **12**(1): p. 011006-011006-7.
13. Clifford, G.D., *Rpeakdetect function (ECG toolbox).* 2008.
14. van Velzen, M.H.N., et al., *Increasing accuracy of pulse transit time measurements by automated elimination of distorted photoplethysmography waves.* Med Biol Eng Comput, 2017. **55**(11): p. 1989-2000.
15. Kaw, A. *Finding the optimum polynomial order to use for regression*. 2008 [cited 2019; Available from: https://autarkaw.org/2008/07/05/finding-the-optimum-polynomial-order-to-use-for-regression/.
16. Nam, D.-H., et al., *Measurement of Spatial Pulse Wave Velocity by Using a Clip-Type Pulsimeter Equipped with a Hall Sensor and Photoplethysmography*. Vol. 13. 2013. 4714-23.
17. Judd, M. and K. Brindley, *8 - SC soldering processes*, in *Soldering in Electronics Assembly (Second Edition)*, M. Judd and K. Brindley, Editors. 1999, Newnes: Oxford. p. 165-186.

Appendix A – Theoretical background

Cardiovascular diseases and arterial stiffness

The human heart, veins and arteries combined are called the cardiovascular system. This organ system is responsible for several important functions in the body, and is probably most well known for the distribution of blood through the body, and with it nutrients, hormones and oxygen. Cardiovascular diseases (CVDs) are the number one cause of mortality worldwide [1]. CVDs include amongst others strokes, heart failure, hypertension and atherosclerosis. Most of these CVDs are related to an increase in the stiffness of the arterial wall, called arterial stiffening [2, 3].

The term arterial stiffening is used to describe a loss of arterial compliance, which is a measure of the artery's capability of changing volume in response to a pressure change inside the artery [6]. Arterial compliance is important in a healthy cardiovascular system, because expansion of the artery during the contraction of the heart, the systole, partly attenuates the systolic pressure inside the artery, and the subsequent contraction propels the blood forward when the heart is at rest during the diastole, as illustrated in Figure 1. When the arterial stiffness increases, the arterial wall does not expand properly, attenuating the systolic pressure less and increasing the propagation speed of the pressure pulse wave (PW). This is the pressure wave in the artery that is generated by the systole, which is comparable to a sound wave [7]. The speed of the systolic PW is called the Pulse Wave Velocity (PWV) [8]. Note that the PWV is not the speed of the blood moving through the vessel.

Pulse wave velocity

The PWV is described between two successive points in the vascular system, and is directly related to the viscoelastic properties of the artery according to the Moens-Korteweg equation, shown in Eq. (1) [6, 9]. Where $E_{inc,vessel}$ is the incremental elastic modulus, a measure of a material's elasticity, of the vessel wall, h_{vessel} is the vessel wall thickness, r_{vessel} is the vessel radius and ρ_{blood} is the blood density.

$$PWV = \sqrt{\frac{E_{inc,vessel} \cdot h_{vessel}}{2r_{vessel} \cdot \rho_{blood}}} \qquad \text{Eq. (1)}$$

As can be inferred from the Moens-Korteweg equation, a higher incremental elastic modulus, thus higher stiffness, results in a higher PWV. Measuring PWV is seen as the gold standard for determining arterial stiffness in patients, also because of its prognostic value beyond traditional CVD risk factors [10]. When the Moens-Korteweg equation is used, the effect of the viscosity of the blood is assumed to be null. This makes the equation applicable to larger arteries, however towards the periphery of the cardiovascular system, influence of blood viscosity on the PWV cannot be assumed null, which makes the equation inapplicable for smaller arteries, according to Hagen-Poiseuille [11].

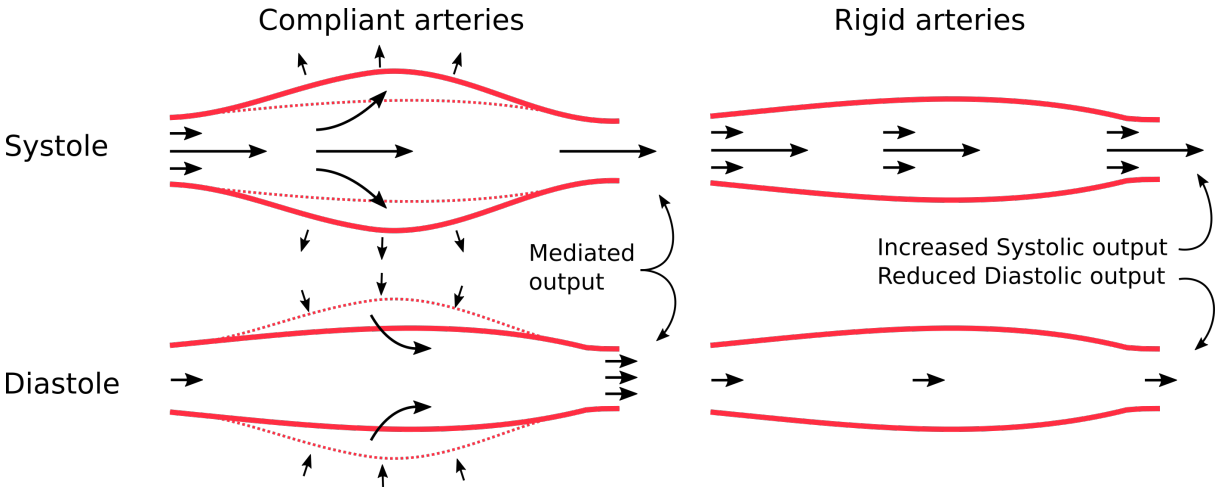

Figure 1 - Difference in blood propulsion between compliant and rigid arteries during systole and diastole. Healthy arteries show expansion and contraction under pressure changes due to volume changes during systole.

Current PWV determination systems

Several devices are currently in use for determining PWV. One of them is the Complior Analyse system (Alam Medical, Saint Quentin Fallavier, France), which measures the Carotid-Femoral PWV, which is the PWV measured between the Carotid and Femoral arteries [12]. To achieve this, piezoelectric sensors are placed on the carotid and femoral arteries. Subsequently, the PWs are detected at these locations and the speed is calculated using the distance between the sensors and the time difference between the arrivals of the PWs at the different locations. The waveforms of these PWs and the carotid-femoral trajectory are schematically shown in Figure 2. PWV along the carotid-femoral trajectory in healthy subjects is between approximately 6 and 10 m/s on average, dependent on age, and can increase to approximately 20 m/s in patients with increased cardiovascular risk [8]. Downsides to the Complior system are that placement of the sensor on the Carotid artery can be experienced as inconvenient and discrepancies between the measured distance between the sensors and the actual distance travelled by the PW might introduces a systematic error in the PWV that is determined [13, 14].

A second system, the Biopac system (Biopac systems Inc., Goleta, California, United States), measures the PWV as the delay between the peak of the ventricular contraction seen in an Electrocardiographic (ECG) signal and the arrival of the PW at a Photoplethysmography (PPG) sensor that is placed on the fingertip. Although placement of the sensors is thought to be less inconvenient than the Complior system, the Biopac system requires the placement of an extra sensor (ECG lead) on the subject, and an educated operator to interpret the two signals, thus still making it a time-consuming and costly process. Additionally, artifacts due to discrepancies between measured distance between sensors and actual path travelled by the PW still might be present, and the actual time between contraction of the heart and expulsion of the PW, called the Pre Ejection Period (PEP) needs to be accounted for, which might make this technique unreliable [15].

Photoplethysmography

The Complior Analyse system uses the technique of PPG to determine the PWV. PPG is an optical measurement technique that is used to detect blood volume changes in vascular tissue [16]. PPG sensors comprise a light source, most often light emitting diodes (LED), and opposing photodiodes (PD), and are placed over a vascularized tissue, such as the fingers, toes, or ears. Water, the main constituent of soft tissue, strongly absorbs light in the ultraviolet and longer infrared wavelengths, and melanin absorbs light with wavelengths shorter than that of red light [16].

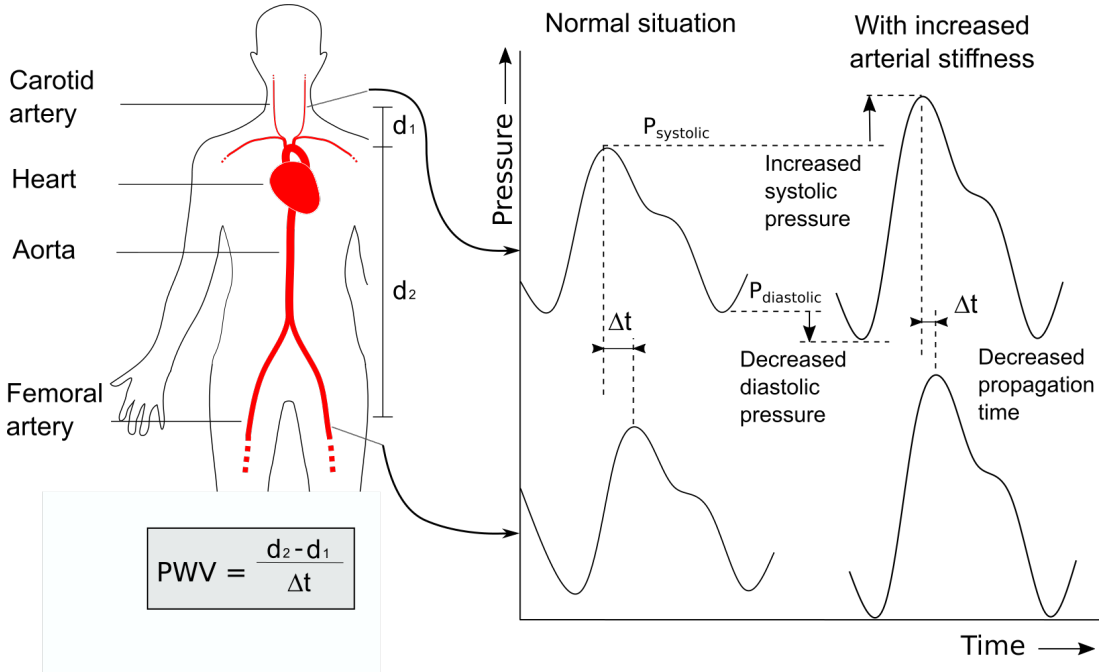

Figure 2 – Representation of the pressure waveforms in the Carotid and Femoral arteries. Also shown is the waveform of the PW with increased arterial stiffness of the Carotid artery. In practise, the pressure inside the stiffer artery is higher but the expansion is smaller, so the PPG signal would have lower amplitude. PWV = Pulse wave velocity. P = pressure.

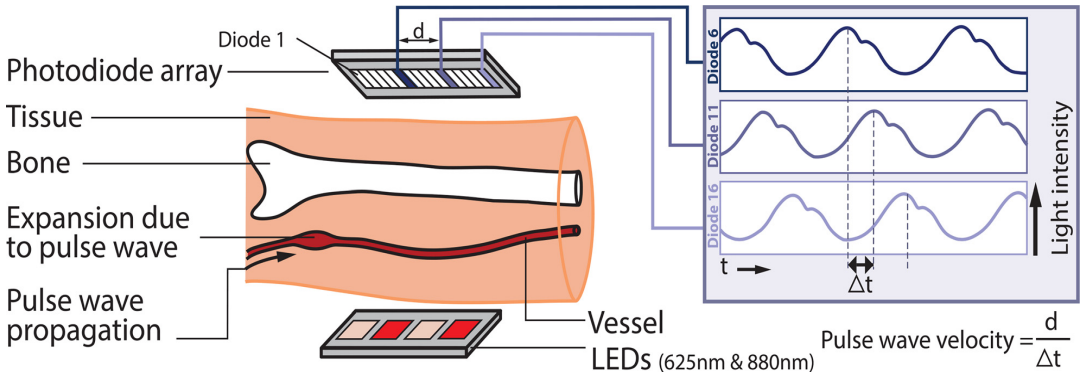

Figure 3 - The MPA as described by van Velzen et al. [5]. Original description: "Fig 1. Schematic overview of the MPA and calculation of the PWV."

Red, near infrared and green radiation are often used in PPG-based sensors and are highly transmissible through soft human tissue. Blood volume changes cause variations in transmissibility of this radiation through the tissue, making it possible for a photodiode to detect changes in blood volume in the tissue. These waveforms can then be used to determine, for example, the pulse rate. Another important clinical feature of PPG is that differences in oxygenation of the blood can be measured. Red light is absorbed more strongly by oxy-hemoglobin (HbO_2) than infrared light [17]. By rapidly switching between red and infrared radiation, the difference in transmission between the two wavelengths can be used to estimate the oxygen saturation of the blood [18]. PPG can be used to determine the PWV because with it, the PW can be 'seen' in the tissue. During the peak of the PW, volumetric expansion of the vessel is greatest, which means it can be directly related to the highest decrease in PPG-signal [19, 20]. When the PPG signal is collected in two locations over a known distance, the PWV can be determined as the distance between the locations divided by the temporal difference between the signals [9].

Multi Photodiode Array

The MPA is a PPG-based sensor developed by M. Van Velzen et al of which published documentation dates back to 2017 [5]. It comprises a row of 16 photodiodes, excited by four opposing LEDs, two red (620nm) and two infrared (880nm). The two parts of the MPA (LED array and PD array) are to be placed on opposite sides of a vascular tissue, after which relative PW propagation can be monitored between photodiodes. The MPA allows for calculation of the PWV over a distance much smaller than the carotid-femoral distance (Figure 2), namely theoretically the distance between two consecutive photodiodes, which in case of the MPA is a mere 0.8mm [5]. This feature provides several benefits over conventional methods. First, the MPA requires the placement of only one sensor unit, as opposed to multiple in other methods, which could minimize the difficulty of accurately placing the sensor, and minimizes discrepancies due to a difference in the distance between the sensors and the actual path travelled by the PW, according to van Velzen et al [5]. Additionally, a small and simple sensor can be applied with less inconvenience to the patient, and would not require experienced operators. The MPA as described by van Velzen et al is schematically shown in Figure 3. Another benefit of the MPA is that it's functionality is based on a technology already in use in common blood oxygenation meters, which can be altered to encompass the new functionality of the MPA without losing it's old function, thus negating the need for additional implementation measures.

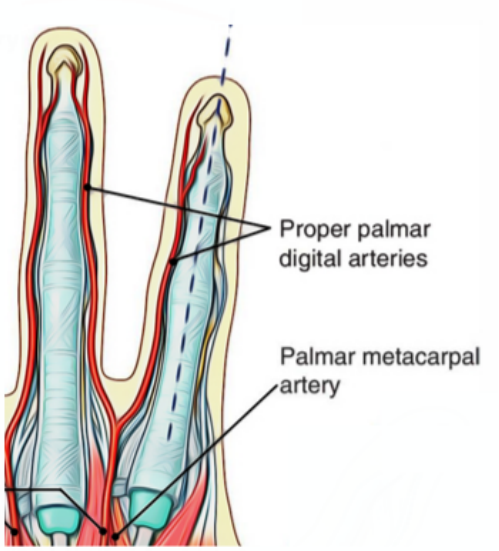

Figure 4 - Palmar view of the right index and middle fingers, showing the proper palmar digital arteries. Image courtesy of Earth's Lab [4].

The MPA was clinically tested to determine the PWV in the proper palmar digital artery (PPDA) of the left index finger, shown in Figure 4. Common blood oxygenation- and heart rate sensors are also commonly applied to this tissue in a clinical setting. Signal robustness of the MPA was tested with several different phalanx placement locations, PD and LED array orientations and with collimators, to attempt to reduce light scatter. Clinical validation of the MPA was performed with surfaces of the PD and LED arrays under a 90 degree angle with respect to one another and placement of the distal phalanx with the palmar side to the LED array, with the PD array aligned with the 'middle, fleshy side part of the distal phalanx and using light contact pressure' [19].

References

1. Roth, G.A., et al., *Global and regional patterns in cardiovascular mortality from 1990 to 2013.* Circulation, 2015. **132**(17): p. 1667-78.
2. Laurent, S., et al., *Aortic stiffness is an independent predictor of all-cause and cardiovascular mortality in hypertensive patients.* Hypertension, 2001. **37**(5): p. 1236-41.
3. Zieman, S.J., V. Melenovsky, and D.A. Kass, *Mechanisms, pathophysiology, and therapy of arterial stiffness.* Arterioscler Thromb Vasc Biol, 2005. **25**(5): p. 932-43.
4. Volker, J.H. *SUPERFICIAL PALMAR ARCH*. 2018 [cited 2019 23-04]; Available from: https://www.earthslab.com/anatomy/superficial-palmar-arterial-arch/.
5. van Velzen, M.H.N., et al., *Design and Functional Testing of a Novel Blood Pulse Wave Velocity Sensor.* Journal of Medical Devices, 2017. **12**(1): p. 011006-011006-7.
6. Gosling, R.G. and M.M. Budge, *Terminology for describing the elastic behavior of arteries.* Hypertension, 2003. **41**(6): p. 1180-2.
7. Cecelja, M. and P. Chowienczyk, *Role of arterial stiffness in cardiovascular disease.* JRSM Cardiovasc Dis, 2012. **1**(4).
8. Boutouyrie, P. and S.J. Vermeersch, *Determinants of pulse wave velocity in healthy people and in the presence of cardiovascular risk factors: 'establishing normal and reference values'.* Eur Heart J, 2010. **31**(19): p. 2338-50.
9. Tijsseling, A.S.A., A., *A. Isebree Moens and D.J. Korteweg: on the speed of propagation of waves in elastic tubes*. 2012: Technisch Universiteit Eindhoven.
10. Willum-Hansen, T., et al., *Prognostic value of aortic pulse wave velocity as index of arterial stiffness in the general population.* Circulation, 2006. **113**(5): p. 664-70.
11. Sucowsky, P. *Cardiovascular Biofluid Mechanics Chapter 4: Mathematical Modeling*. 2016 [cited 2019 25-05-19]; Available from: http://www.wright.edu/~philippe.sucosky/ME7370.html.
12. *Complior PWV info center*. [cited 2018 20-06]; Available from: http://www.complior.com/info-center.
13. van Velzen, M.H.N., et al., *Comparison between pulse wave velocities measured using Complior and measured using Biopac.* Journal of Clinical Monitoring and Computing, 2018.
14. Townsend, R.R., et al., *Recommendations for Improving and Standardizing Vascular Research on Arterial Stiffness: A Scientific Statement From the American Heart Association.* Hypertension (Dallas, Tex. : 1979), 2015. **66**(3): p. 698-722.
15. Balmer, J., et al., *Pre-ejection period, the reason why the electrocardiogram Q-wave is an unreliable indicator of pulse wave initialization.* Physiol Meas, 2018. **39**(9): p. 095005.
16. Allen, J., *Photoplethysmography and its application in clinical physiological measurement.* Physiol Meas, 2007. **28**(3): p. R1-39.
17. Gordy, E. and D.L. Drabkin, *Spectrophotometric studies. XVI. Determination of the oxygen saturation of blood by a simplified technique, applicable to standard equipment.* J Biol Chem, 1957. **227**(1): p. 285-99.
18. Clark, T. *Pulse Oximetry*. 2011 [cited 2018 26 September 2018]; Available from: http://its.uvm.edu/medtech/Tmodule.html.
19. van Velzen, M.H.N., *The Speed Of Waves - Measuring the velocity of pressure pulse waves traveling through blood in the peripheral blood vessels*. 2019, Erasmus Universiteit Rotterdam.
20. Vlachopoulos, C.O.R., M.; Nichols, W.W., *McDonald's Blood Flow in Arteries Theoretical, Experimental and Clinical Principles*. 6 ed. 2011, London.

Appendix B - Statement of requirements and preferences and technical translation

First, the intended use of the device and its functionality is summarized, which is then translated into the main functional characteristics. These functional characteristics are achieved through the subsequent technical specifications, which are then addressed individually.

Device description and intended use

The sensor that is to be designed is a miniature transmission Photoplethysmography-based (PPG) sensor based on the measurement technique applied in the Multiphotodiode Array (MPA). Therefore a lot of requirements are adapted from the work of van Velzen or stem from the basis of the technique of PPG [1-3]. The sensor is to be incorporated in a device in which the contact pressure between the sensor and the vascularized tissue can be altered and quantified. The device is to be used to safely and accurately determine the optimal contact force for accurate determination of the Pulse Wave Velocity (PWV) in the peripheral vasculature of the distal phalanges of all fingers but the thumb of multiple test subjects in a non-clinical setting. To concretize:

The device is a PPG-based sensor with alterable and determinable contact force for accurate and safe determination of the PWV in the vasculature of the distal phalanges of multiple test subjects.

The description can be translated to six main functional characteristics:

1. **PPG basis** - The sensor is based on the technology of PPG.
2. **Contact force** - Contact force between the sensor and the vascularized tissue can be adjusted and this adjustment can be quantified.
3. **Signal generation and processing** - The sensor generates signals from which the PWV in the tissue can be determined.
4. **Accuracy** - The signal that is generated by the sensor is continuous and not deteriorated by component specifications or electrical and/or structural integrity.
5. **Safety** - The device is not harmful to user or test subject under normal operating conditions relating to force range experimentation.
6. **Placement and applicability** - The device is able to fit the healthy distal phalanges of all fingers (but with minimal importance for the thumb) of a large human population.

Functional translation of device description

The seven main functionalities need to be achieved through the technical specifications of the sensor. Each of the main functionalities is further addressed and the necessary technical requirements are further specified.

1. PPG basis

The sensor has to be capable of detecting blood volume changes thus the working principle and underlying technique is based on PPG.

1.1 PPG-based signal generation

The sensor is to be based on PPG, which means that the sensor comprises an (near-) infrared light source and an opposing photodiode (PD) unit that can pick up (near-) infrared wavelengths [1].

1.2: Led wavelength

For ideal signal generation, the light emitting part of the sensor should emit light around 805 nm since this wavelength is ideal to measure human blood volume changes [1]. This is achieved by using 2 near infrared LEDs with peak emission at 850nm (HT-170IRPJ, Harvatek, Hsinchu City, Taiwan).

1.3: Peak sensitivity photodiode unit

To ensure high PPG signal intensity, the peak sensitivity of the PD unit should lie around that of the wavelength of the light that is transmitted by the LEDs [1]. Therefore, SI-PIN PDs with a peak sensitivity at 850nm are used (SFH 2400, OSRAM Opto semiconductors GmbH, Regensburg, Germany).

2. Contact force

The contact force between the sensor and the vascularized tissue of the subject should be adjustable and determinable.

2.1: Alterable sensor contact force

The contact force between the sensor and tissue should be adjustable in the device so that dependency of PPG signal robustness on contact force can be studied. This is achieved by incorporating a linear stage over the sensor, to which a weight holder is attached that is placed onto the finger. The weight holder can hold differing weights.

2.2: Determinable sensor contact force

To be able to quantify the dependency of PPG signal robustness on contact force of the sensor with the tissue, real-time contact force should be determinable for each situation. This is achieved by placing the linear stage and sensor onto a scale, of which the weight can be read. All forces run through the interface between the finger and sensor, thus the weight measured can be recalculated between the absolute contact force between the sensor and the finger.

3. Signal generation and processing

The device should generate multiple signals from which the PWV can be determined. The working principle and underlying technique are adapted from the MPA, validated by van Velzen [4].

3.1 Multiplicity of photodiodes

For the PWV to be determined a multitude of PDs should be incorporated in the sensor. The use of 4 PDs is adapted from the validation by van Velzen [2]. These PDs are be placed at known distances from each other, along the path of the PW.

3.2: PWV calculation

A program written for data processing and accurate determination of the PWV is available and has been validated by van Velzen [2]. This program shall be used for further testing and will be adapted to the new experimental sensor.

4. Accuracy

Signal robustness was found to be dependent on contact force of the sensor with the skin of the test subjects and on movement artifacts [4]. PWV accuracy is also dependent on processing (and subsequent elimination) of distorted signals, either caused by physiologic parameters, or signal processing errors.

4.1: Alterable sensor contact force (duplicated from 2.1)

4.2: Angle between diode and LEDs

In the last clinical validation, van Velzen found that an angle of 90 degrees between the surfaces of the PD and LED arrays provided sufficient signal transmission [4]. To preserve the influence of these specifications the angle between the PD and LED arrays are placed under this angle with respect to one another in the experimental sensor.

4.3: Sampling frequency

To optimize data reliability, the sampling frequency should be sufficient to accurately detect the peaks of successive PWs, and preferably as high as possible. Key for this requirement is that the photodiode 'notices' the peak of the pressure wave as it passes by it's photoactive surface. This means the signal should be sampled at least once during this period. This means the sampling frequency should at least equal the maximum PWV to be measured, divided by the width of the photoactive surface in the direction of the path of the PW. According to the Nyquist theorem the actual sampling frequency should be at least two times this, and preferably as high as possible. The analog-to-digital conversion card has a maximum sampling frequency of 250 kHz. This means that each PD can be read out with a max sampling frequency of 62.5 kHz. According to Eq. (1) this is sufficient to accurately sample PWV's up to 31,25 m/s. Since it is highly unlikely to encounter PWVs over 20m/s and are more likely to be around 0.8m/s [2, 4-6].

$$f_{min} = (2 * PWV_{max}) / \, l_{pd} \; [Hz] \qquad \text{Eq. (1)}$$

In Eq. (1), $f_{min}$is the minimally required sampling frequency in Hz, PWV_{max} is the maximum PWV that is to be measurable with the sensor in meters per second and l_{pd} is the length of the path travelled by the PW along the photoactive surface of the PD in meters.

4.4: Signal filtering

Distorted PW measurements are found to cause wrong PWV outcomes, which need to be avoided [3]. Distorted and/or unusable PWs are eliminated from further calculation, increasing robustness of the PWV outcomes. For this, the '7Step PW-filter' algorithm developed by van Velzen is used [3]. This algorithm uses Boolean algebra to eliminate distorted PW signals from the dataset, and excludes them from PWV calculations.

4.5: Number and placement of LEDs

The number of LEDs should provide sufficient coverage over the PDs such that intensity of radiation that reaches the PDs generates a clear signal. Furthermore, to ensure proper transmission through the tissue and minimize light scatter, the LEDs should be placed at the same location along the path of the PW as the PDs, so that they shine directly at them. To achieve this, two infrared LEDs are used that are aligned such that the first infrared LED, seen in the direction of travel of the PW is directly in the middle of PD 1 and 2, and the second LED is directly in the middle of PD 3 and 4.

4.6: Number of Photodiodes

Theoretically, PWV can be calculated using signals from only two PDs, however, a higher number of PDs provides the possibility for calculation of PWV over $(n-1)!$ intervals, where n is the number of PDs. Due to size restriction of the PD array posed by phalange size, also mentioned under section 7.3: 'PD array size', the number of PDs that is to be incorporated into the sensor unit is four. A combination of four photodiodes has been tested by van Velzen during functional testing of the MPA and was found reliable [2].

5. Safety

To ensure safety of all who come into contact with the device, several precautions should be taken to ensure no physical harm is induced. The device is designed and constructed to conform to CE guidelines. Additionally, some points are taken into special consideration.

5.1: Tactile safety

Sharp edges on which the test subject, experimenter or anyone from the production process onward could injure itself, are removed from both the sensor and the linear stage. Furthermore, gaps and crevices on which the skin could be pinched are minimized.

5.2 Electrical safety

Levels of electricity are to be kept at a minimum for the sensor to still function, also reducing the risk of electrifying the test subject or the experimenter. The forward voltage used by the sensor is 5V, taking that the resistance of dry human skin is 100.000 Ohms, the maximum current through the skin is 0.05mA, which is at a safe level [7]. Furthermore, all electrical components in the sensor should be properly shielded from contact.

5.4: Cleanability

To ensure subject safety the sensor should be cleanable if necessary. The 3d printed casing and upper surfaces of the PD and LED arrays were wiped down with high alcohol content lens cleaning tissues (Swirl Clean Glasses, Melitta Group, Minden, Germany).

6. Placement and applicability

To ensure a broad employability of the sensor during experimentation, placement location and fixation should be determined and remain static during experimentation.

6.1 Placement location

The experimental setup designed by van Velzen was designed to measure PWV in the PPDA in the distal phalange of the index finger [4]. To ensure flexibility for application of the sensor, the choice was made to make the design applicable to all distal phalanges with minimal importance for the thumb, since the distal phalange of the thumb was thought to differ geometrically from other phalanges more often. The placement of the distal phalanx of the left index finger was prescribed in the measurement protocol.

6.2 Sensor geometry

During clinical validation, van Velzen placed the LEDs on the bottom side of the finger, and the MPA on the side [4]. This configuration will also be applied in the new experimental sensor. The exact placement of the PD array will be chosen so that the centerline of the array is exactly placed at half the height of the smallest finger of the author, the little finger of the left hand (5.5mm). The exact placement of the LED array will be chosen so that the centerline of the LED array is exactly positioned at half the width of the smallest finger of the author (6.1mm).

6.3: Placement fixation

The location of the sensor with respect to the distal phalange of the test subject should remain the same during the experiment. Movements may cause artifacts and compromise signal robustness. Therefore it is incorporated into the measurement protocol that the subject remains still during the measurement.

6.4: Photodiode array size

Buryanov et al. reported on hand segment measurements of 66 people without bone pathology or deformities [8]. To ensure that all PD's are covered during use of the device, the PD array size should not exceed the shortest measured length of the largest phalange. It was found that the distal phalange of the middle finger measured 17.4 ± 1.85 mm (mean ± SD)[8]. Therefore the length of the PD array should not exceed 13.7mm. With the currently used PD modules, the length of the PD array is 10.2

Additional preferences

However not technically stringent, the placement of the PDs is kept modular, so different configurations of PDs and LEDs can be tested using the same experimental sensor. Furthermore, modularity allows for quick replacement of specific sensor components when these are broken or malfunction, or other configurations or component specifications are desired.

References

1. Allen, J., *Photoplethysmography and its application in clinical physiological measurement.* Physiol Meas, 2007. **28**(3): p. R1-39.
2. van Velzen, M.H.N., et al., *Design and Functional Testing of a Novel Blood Pulse Wave Velocity Sensor.* Journal of Medical Devices, 2017. **12**(1): p. 011006-011006-7.
3. van Velzen, M.H.N., et al., *Increasing accuracy of pulse transit time measurements by automated elimination of distorted photoplethysmography waves.* Med Biol Eng Comput, 2017. **55**(11): p. 1989-2000.
4. van Velzen, M.H.N., *The Speed Of Waves - Measuring the velocity of pressure pulse waves traveling through blood in the peripheral blood vessels*. 2019, Erasmus Universiteit Rotterdam.
5. Boutouyrie, P. and S.J. Vermeersch, *Determinants of pulse wave velocity in healthy people and in the presence of cardiovascular risk factors: 'establishing normal and reference values'.* Eur Heart J, 2010. **31**(19): p. 2338-50.
6. Nam, D.-H., et al., *Measurement of Spatial Pulse Wave Velocity by Using a Clip-Type Pulsimeter Equipped with a Hall Sensor and Photoplethysmography*. Vol. 13. 2013. 4714-23.
7. *WORKER DEATHS BY ELECTROCUTION A Summary of NIOSH Surveillance and Investigative Findings*. 1998, U.S. DEPARTMENT OF HEALTH AND HUMAN SERVICES.
8. Buryanov, A.K., V., *Proportions of hand segments.* International Journal of Morphology, 2010. **28**(3): p. 755-758.

Appendix C – FA-MPA design process

This document describes the three design paths that were discarded for three main characteristics of the FA-MPA. First, the reason why a portable experimental sensor was not deemed feasible is addressed. Then, the choice to discard the option to alter and determine the contact force per individual photodiode is addressed, after which an explanation is given as to why electrical sensors and force normalization were discarded. Finally, a more detailed explanation of the idea of force normalization for individual photodiodes (PDs) is given, to provide a handle for future design iterations into a force normalized sensor.

Combination of functionalities – portable experimental sensor

In an early stage of the experimental design, possibilities were investigated to combine the functionalities of the experimental device with the characteristic of portability of a clinical prototype. The main idea behind this combination was that not only could the device then be used for contact force experimentation, the same functionality could eventually be implemented for contact force alteration in the future clinical setting if needed. It was thought that design features that made alteration or normalization of sensor contact force possible could also help improve the applicability of the device on tissues other than the distal phalanges of the fingers since force discrepancies due to tissue elasticity or geometry could be omitted by the alterability of the mechanism. Mechanisms for force alteration and determination that were opted were: 1. A displacement screw with a miniature force sensor, screwed into the casing up to an exact contact force with the skin, using the skins own elasticity 2. A pneumatic or hydraulic system with a bellow that could be pressurized to press the PDs into the skin in combination with a pressure sensor inside the bellow or inside the tubing; 3. A ratchet system with which the sensor could be ratcheted only up to a certain point of maximum contact force, after which the mechanism would 'shoot through'; 4. A preloaded (double) spring with very low spring constant, such that the spring theoretically exerts a force between 2.95 and 3.05 at the minimum and maximum extension, related to 5^{th} and 95^{th} percentile of finger thickness; 5. A statically balanced system, also called a constant force mechanism. Sketches of the proposed systems are shown in Figure 1. The statically balanced system, or constant force mechanism, is further elaborated upon under the subsection 'Contact force sensing and normalization – Contact force normalization'.

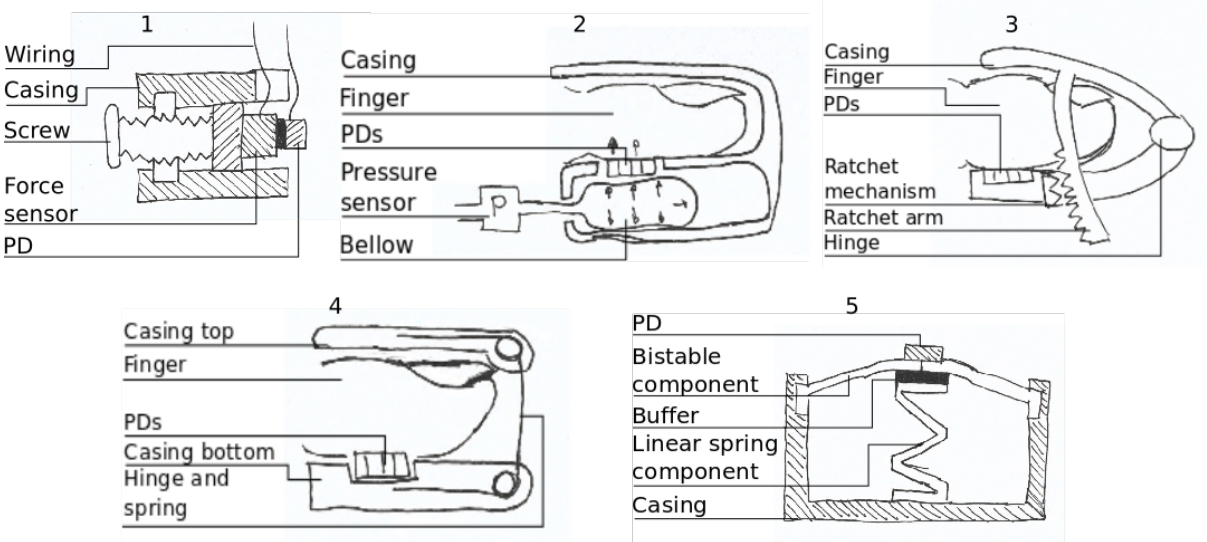

Figure 1 – Sketches of early design options. 1: Single unit with electrical force sensor and set screw. 2: Hydraulic/pneumatic option with bellow. 3: Ratchet mechanism. 4: Hinge and spring under pretension. 5: Single unit with constant force mechanism. PD is photodiode.

For the sensor to be portable like common clip-like pulse-oximeters often found in clinical settings, the mechanisms had to be miniaturized as to take up as little space in the sensor and to reduce overall weight. Moreover, experimentation into contact force dependency required a high accuracy in contact force alteration and determination. Achieving both portability and high accuracy was perceived too difficult to achieve in the time scope of this research, and was subsequently abandoned. Instead, the choice was made to primarily focus on an experimental setup for high accuracy contact force determination after which concluding data on preferable sensor contact force could be used in the design of a functional prototype.

Individual photodiode contact force

Early in the project, possibilities were sought for altering and determining the contact force per individual photodiode. The main reason for this was to accommodate the curvature of the finger and mitigate the presumed impact of highly local deviation of soft tissue physiology and the irregular shape of the osseous tissue in the distal phalanx. The same arguments were made against this design option as were made against portability of the experimental sensor; It was deemed technically too difficult since force alteration and determination mechanisms had to be even further miniaturized than with a portable sensor which was thought to make the application of a contact force alteration mechanism even more difficult. Research was performed into contact force normalization instead of alteration per photodiode using an adjustable constant force spring mechanism, which is elaborated on under the subsection 'Contact force sensing and normalization – Contact force normalization' in this appendix, but this option was also discarded. Although this design and research path was discarded, it might still prove useful to seek out if contact force generated per individual photodiode could improve signal robustness. This could be done by means of assessing the quality of the peak detection or correlating the individual contact force to the number of discarded signals by the '7-step-PW-filter' and the reason why they were discarded [2]. This would ask for a novel experimental setup that is specially designed for this function, which is presumably feasible, but did not fit the time scope of the current research.

Contact force sensing and normalization

Electrical sensor equipment
During the initial course of seeking options to determine the optimal contact force per individual photodiode, it was sought out to determine the contact force between the distal phalanx and the MPA by means of electrical sensors for example piëzoresistors and load cells. However, the dimensions of the sensors currently on the market that were found by the author were too large to be incorporated in the device making it difficult for the dimensional requirements to be met. However, if signal robustness could be improved until the point that the two last photodiodes in the array become obsolete (number of signals filtered from PD 1 and 2 becomes negligible), space might be available for miniature force sensors in combination with a force alteration mechanism. Incorporating pressure sensors in combination with miniature pressurized bellows investigated but subsequently discarded because it was deemed mechanically too difficult and inaccurate. Incorporation of flexible force sensors was also investigated, but subsequently discarded because it was thought these would be too large and would be too inaccurate to force components perpendicular to the contact area between the sensor and the distal phalanx.

Contact force normalization
After veering off the path of electrical force sensors, the option of contact force normalization for individual PDs was investigated. Moreover, the possibility of implementing a constant force mechanism (CFM) was researched. A CFM is a mechanism that uses a combination of a linear spring and a bistable mechanism to create an interval of compression in which the compression force is constant. A bistable mechanism has a positive spring constant at the start of the deformation, but changes to a negative spring constant after the 'snap-through point'. The deformation of a singular bistable beam and its force-deformation curve are shown schematically in Figure 2. A CFM uses a bistable mechanism in combination with a linear spring mechanism. The effective spring constant becomes that of both spring constants combined.

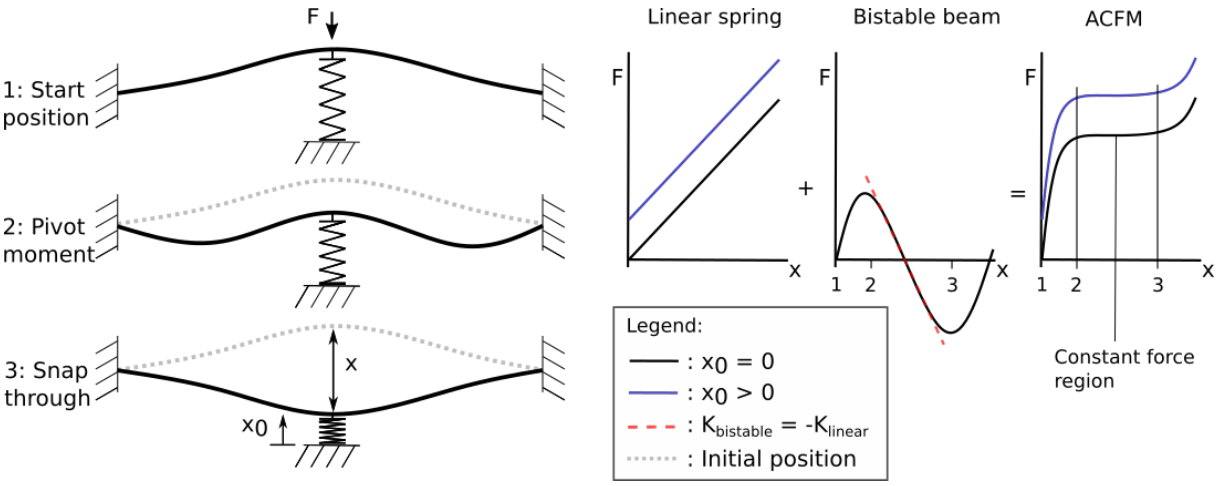

Figure 2 - Schematic representation of an Adjustable Constant Force Mechanism. The figure shows the deformation of a singular bistable beam and a linear spring. The graphs show the force-displacement for the individual systems, and the two systems combined.

If dimensioned properly, the positive spring constant of linear spring will now exactly counteract the negative spring constant of the bistable mechanism, functionally providing a mechanism with zero stiffness over a certain increment of compression distance, called the 'constant force region'. Lan et al. experimented with altering the pretension of the linear spring, effectively generating an Adjustable Constant Force Mechanism (ACFM), in which the plateau of constant force could be altered according to the application's needs, as is represented in blue in Figure 2 [3].

The main challenge in designing an ACFM for such a specific purpose is to dimension a mechanism of which the force/displacement curve exactly fits the process needs. This is particularly difficult for structures in which deformations are nonlinear, which is the case in ACFMs. For the FA-MPA this meant that an adjustable normalized force of 1-4N was needed, with a maximum compression directly related to the fingertip stiffness [1]. For the research of Lan et al., a script written in MATLAB was used for the optimization of the ACFM shape and dimensions [3]. At first, it was attempted to recreate such a script for the current research into PD contact force. However this was deemed not feasible in the current time schedule and unfortunately the authors of the original script were reluctant to provide it. Thus, the possibility of iteratively designing an ACFM mechanism using computer simulation software was investigated. Unfortunately, abundant and long lasting technical difficulties and incompatibilities with a number of programs (COMSOL Multiphysics, Abaqus, Solidworks, ANSYS AIM) greatly reduced the feasibility of this design option. These problems mainly included unavailability of software licenses, insufficient functionalities of the software (missing toolboxes, inaccurate simulations due to very low number of finite element model nodes) and software malfunctions due to wrongful installation. Thus the choice was made to also discard this design option, and seek a solution in quantifying contact force between the experimental sensor and the tissue, rather than normalizing it.

The force-displacement curve of a Miniaturized ACFM (MACFM) could be made manually, by simulating a static displacement of the top of the MACFM by several increments, plotting these values against the subsequent reaction forces of the system and interpolating to create the force-displacement curve. This was to be done using the predefined geometry determined by Lan et al. and structural dimensions obtained by scaling the moment of inertia of the inner components to match force and dimensional specifications for the FA-MPA. However, manually obtaining the values for the reaction force under known compression would require several simulations per design iteration, thus this was deemed too tedious and time-consuming. The main challenge in this process was, and is still, to design and dimension a mechanism that behaves such that the MACFM provides the right contact pressure between the photodiode and the tissue, regardless of what the decompression of the photodiode and underlying mechanism is. This makes that the MACFM mitigates any irregularities in tissue physiology, and with that it's geometry and elasticity, ensuring that the contact force is always identical for each photodiode. The way in which two diodes, both supported by an MACFM, would react to a tissue with non-linear stiffness at different contact forces is shown schematically in Figure 3.

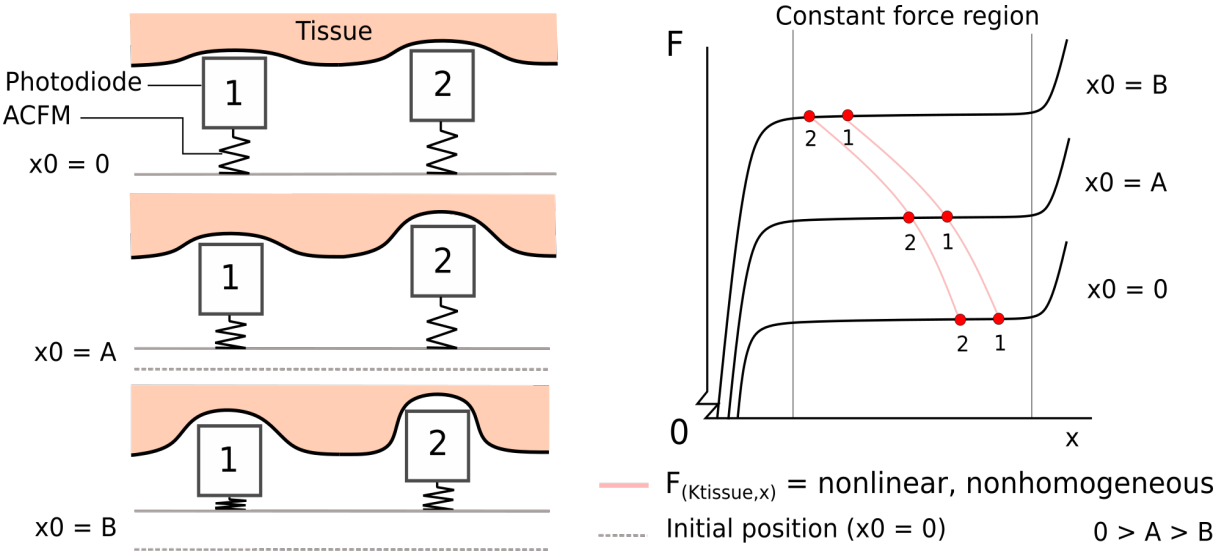

Figure 4 - MACFM deflection under different values for x0 (spring pre-displacement) and with nonhomogeneous tissue characteristics. $F_{(Ktissue,x)}$ = nonlinear according to Han et al [1].

Another design difficulty was that the forces generated by the mechanism were small, thus also greatly decreasing the mechanism dimensions. This meant that adding electrical contacts to the photodiodes would increase the linear spring constant of the system, making it more difficult to find a suitable bistable mechanism that could counteract this spring constant. Therefore it was reasoned to try and incorporate both functionalities (bistable mechanism and electrical conductance) into two bistable beams at either side of the PD. Thus, the electrical contacts *become* the bistable beams. A visual representation of the MACFM that was to be tested is shown in Figure 4. Figure 5 and Figure 6 show the results of a simulation where the top of the MACFM is placed under a 2N load. Figure 5 shows that the stiffness of the structure of 1 N/mm roughly coincides with the stiffness of the tissue in the distal phalanx that was found by Hyun-Yong [1] The structure was considered to be monolithic since accuracy of the simulation was not considered critical for the sole purpose of visualization. Important to notice is the high von Mises stress in the MACFM, which needs to be closely monitored as transcending the yield strength will result in structural failure of the mechanism. This poses another design challenge for the correct design of the MACFM.

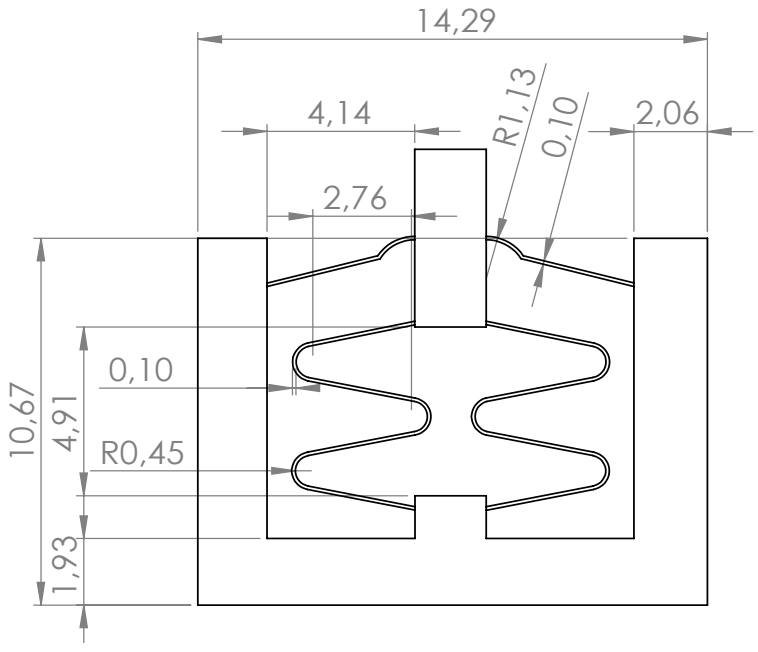

Figure 3 – Drawing of the monolithic MACFM. Measurements are in mm.

Static balancing in a MPA-based device might still be a valuable option for future design iterations, because it negates the necessity of a force 'range' when working with differently dimensioned or characterized tissues the sensor is being used on. For example, a sensor designed to go on the fingertip could be used on fingertips of all dimensions and stiffnesses, given the restraint that the outermost values of those parameters lie within the constant force region of the mechanism. It is strongly recommended that this possibility is further investigated for feasibility and effectiveness for future use, not only in a MPA-based device but possibly for a larger range of devices that might benefit from a force-normalized structural basis and that are used on different tissues such as sonographs, rehabilitation devices to help normalize muscle excitation force or possibly even interventional devices such as tissue clamps [4-6].

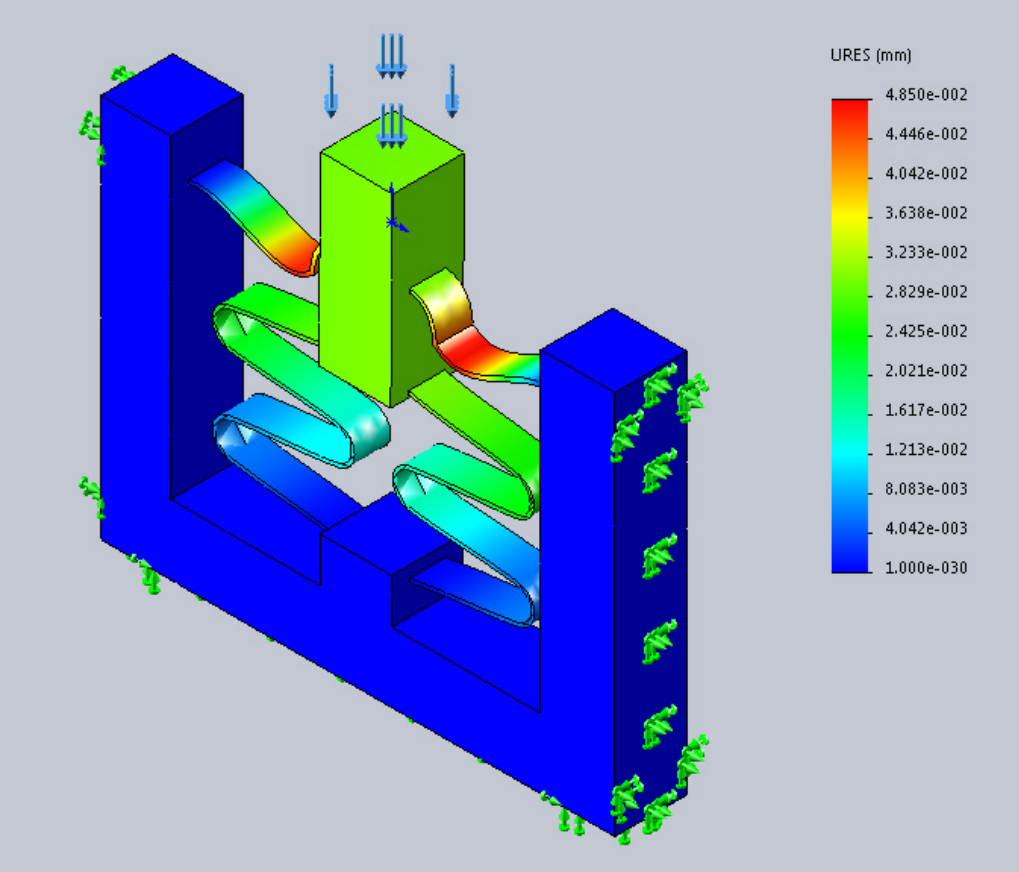

Figure 5 - Displacement of the hypothetical diode module in a MACFM loaded under 2N force.

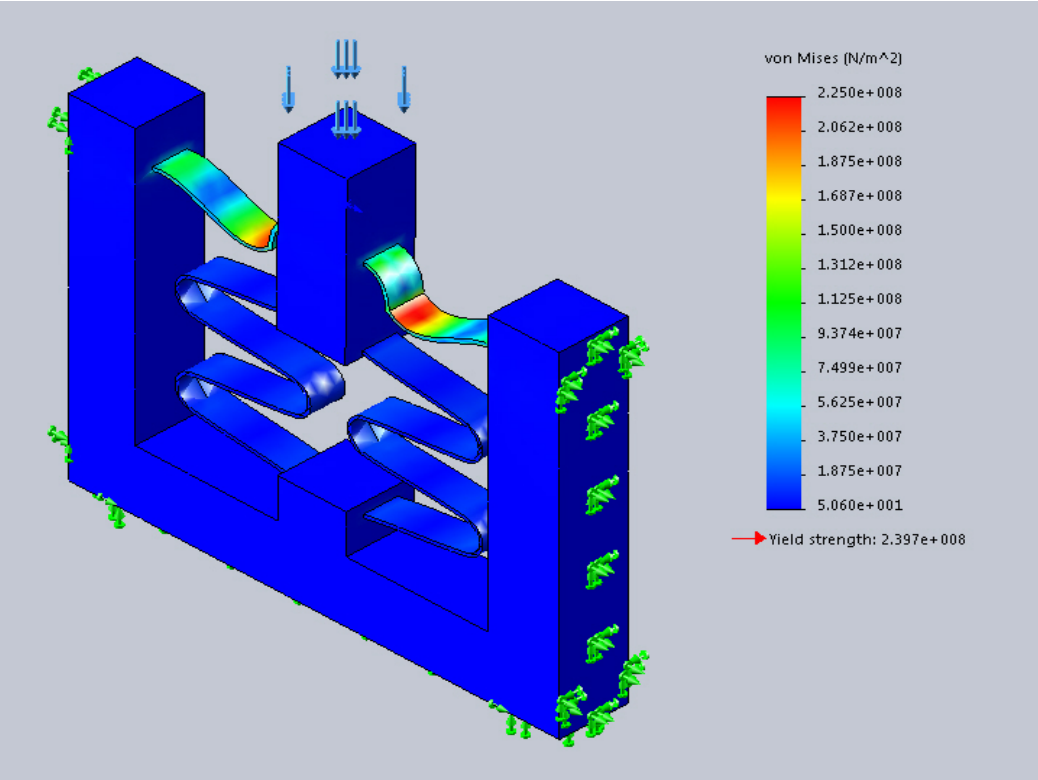

Figure 6 - Von Mises stress in a MACFM loaded under 2N force.

References

1. Hyun-Yong, H. and S. Kawamura. *Analysis of stiffness of human fingertip and comparison with artificial fingers*. in *IEEE SMC'99 Conference Proceedings. 1999 IEEE International Conference on Systems, Man, and Cybernetics (Cat. No.99CH37028)*. 1999.
2. van Velzen, M.H.N., et al., *Increasing accuracy of pulse transit time measurements by automated elimination of distorted photoplethysmography waves.* Med Biol Eng Comput, 2017. **55**(11): p. 1989-2000.
3. Lan, C., J. Wang, and Y. Chen. *A compliant constant-force mechanism for adaptive robot end-effector operations*. in *2010 IEEE International Conference on Robotics and Automation*. 2010.
4. Ihnatsenka, B. and A.P. Boezaart, *Ultrasound: Basic understanding and learning the language.* International journal of shoulder surgery, 2010. **4**(3): p. 55-62.
5. Barone, G.W., et al., *Assessing clamp-related vascular injuries by measurement of associated vascular dysfunction.* Surgery, 1989. **105**(4): p. 465-71.
6. Babin-Ebell, J., et al., *Influence of clamp duration and pressure on endothelial damage in aortic cross-clamping.* Interact Cardiovasc Thorac Surg, 2010. **10**(2): p. 168-71.

Appendix D – Technical documents

The entire electrical infrastructure of the FA-MPA experimental setup consists of four main parts: 1. The FA-MPA sensor; 2. The sensor cable; 3. The data acquisition system; 4. A computer. The first two parts, the FA-MPA sensor and the sensor cable, were specially fabricated for this study. This appendix contains the electrical infrastructure of these two components, as well as their schematics. Furthermore, this appendix contains the technical drawings of the 3D-printed components of the FA-MPA, as well as the assembly drawing.

Electrical infrastructure

Table 1 - Electrical connections between the sensor comonents and the data acquisition system. The intermediate connector is a combination of a TE connectivity female (sensor side) and male (sensor cable side) connector. Strand colors are as seen in an unmarked length of 14-core shielded cable.

Sensor terminal	***Intermediate connector pin no.***	***Strand color***	***D-connector pin no.***
Photodiode 1 Anode	1	White / Black	8
Photodiode 2 Anode	2	Green / Black	6
Photodiode 3 Anode	3	Red / Black	4
Photodiode 4 Anode	4	Orange	2
Photodiode Cathode	5	Black	17
Led Infrared Anode	8	Green	23
Led Hyperred Anode	9	Red	24
Led Cathode	10	Black	25

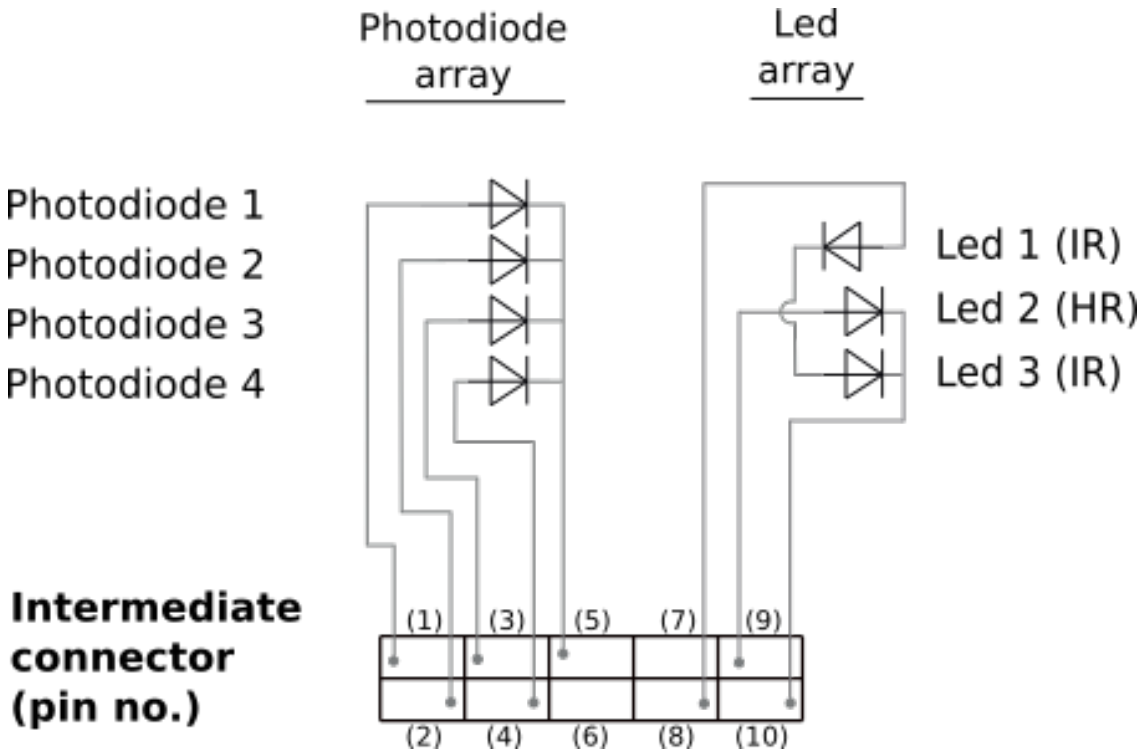

Figure 1 - Electrical infrastructure of the FA-MPA sensor. IR is infrared. HR is hyper red.

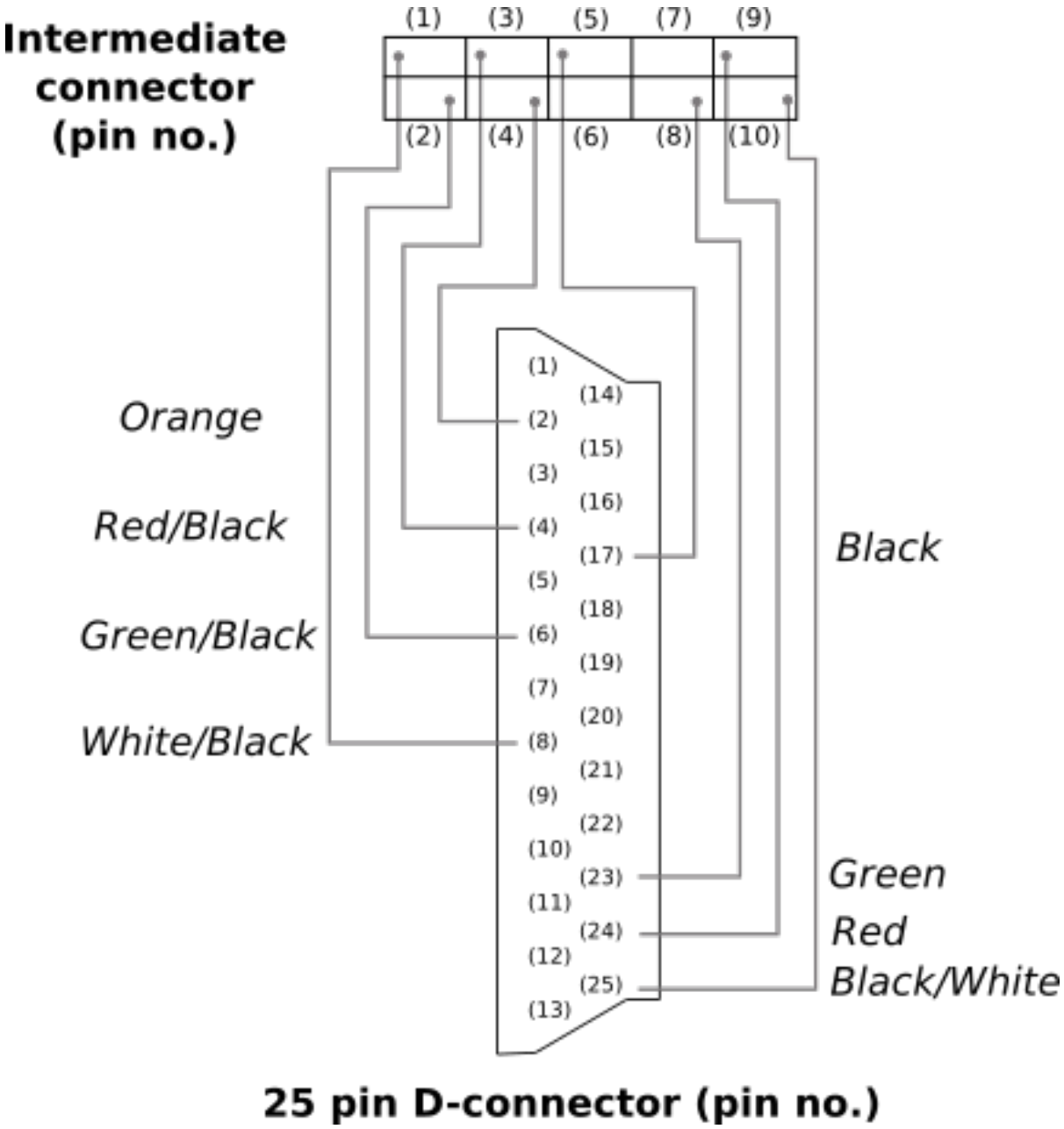

Figure 2 – Electrical infrastructure of the sensor cable. Strand colors are printed in italic.

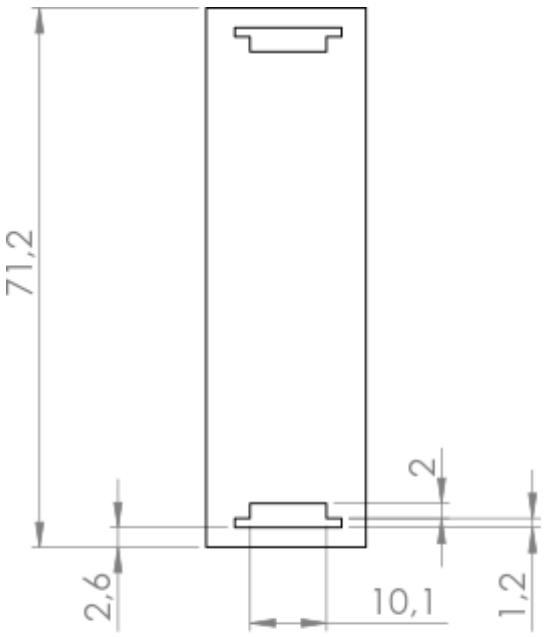

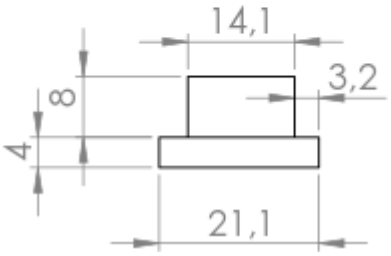

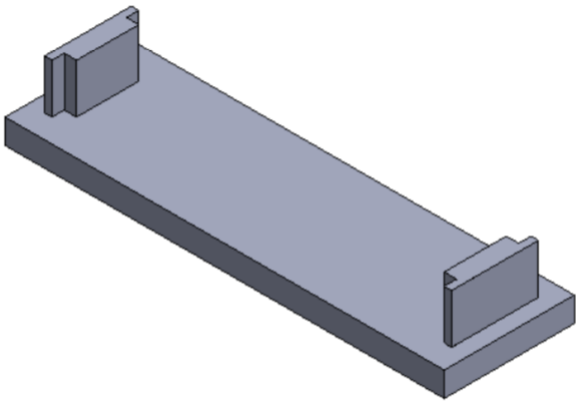

MATERIAL:	PLA BLACK
DIMENSIONS ARE IN MM	
TITLE: LINEAR STAGE TOP	
AUTHOR: M. Adriaanse	A4
SCALE: 1:1	SHEET 1:1

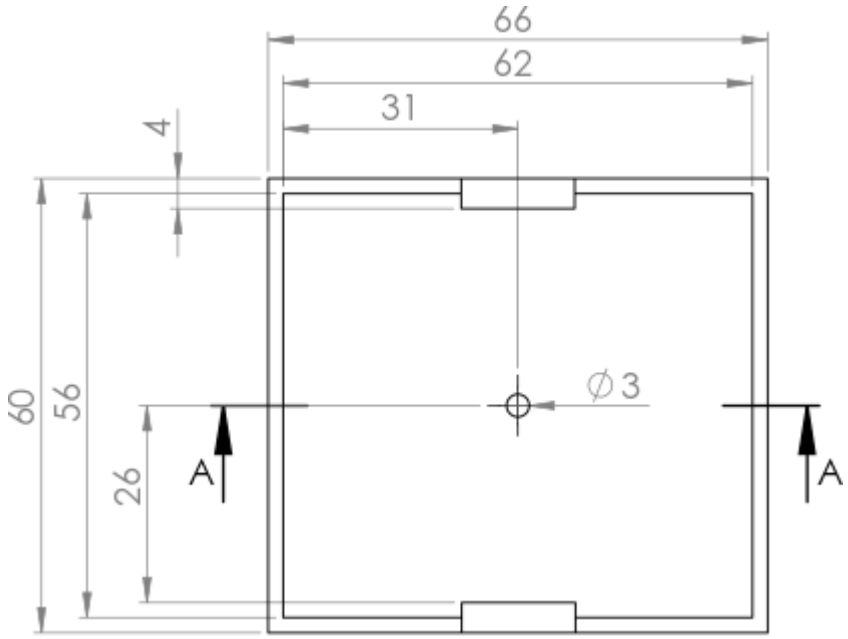

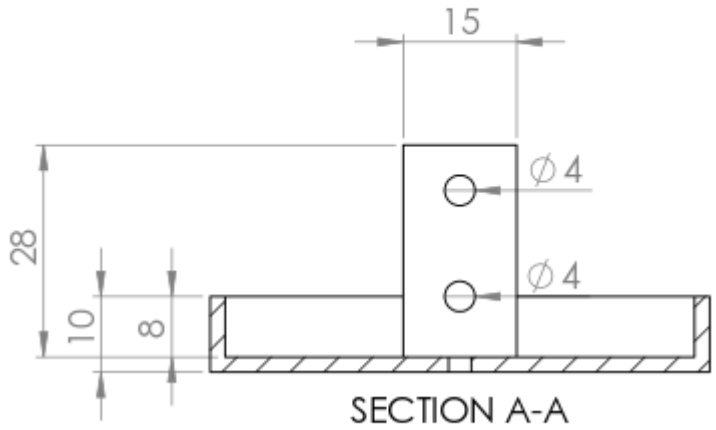

SECTION A-A

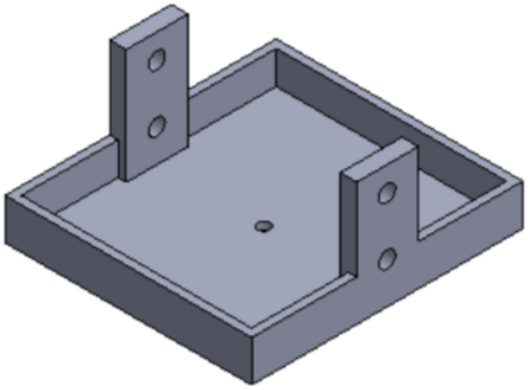

MATERIAL:	PLA BLACK
DIMENSIONS ARE IN MM	
TITLE: WEIGHT HOLDER	
AUTHOR: M. Adriaanse	A4
SCALE: 1:1	SHEET 1:1

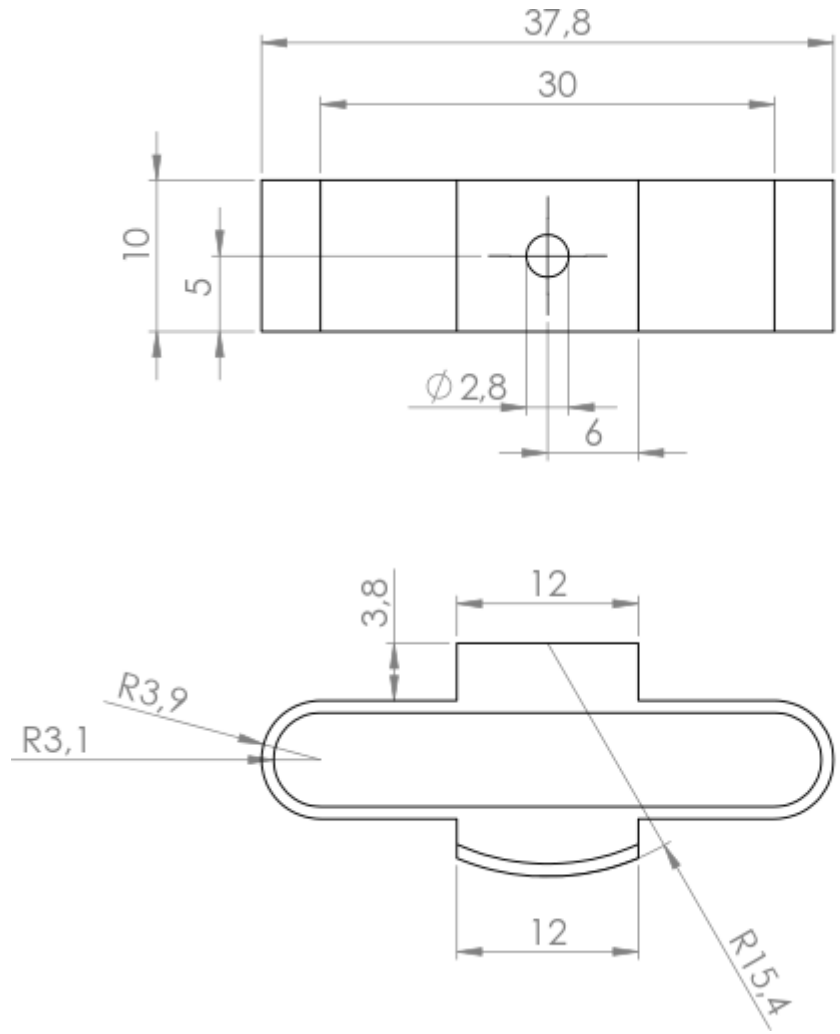

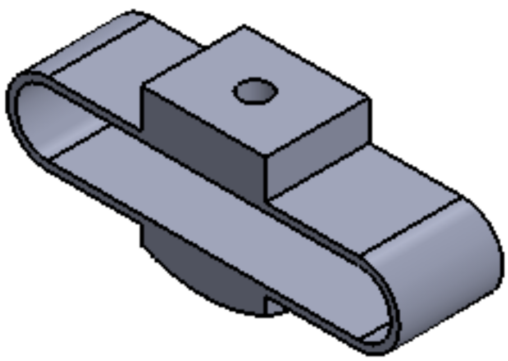

MATERIAL:	PLA BLACK
DIMENSIONS ARE IN MM	
TITLE: CARDANIC SUSPENSION	
AUTHOR: M. Adriaanse	A4
SCALE: 1:2	SHEET 1:1

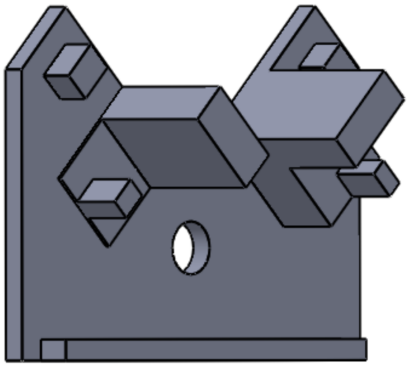

MATERIAL:	PLA BLACK
DIMENSIONS ARE IN MM	
TITLE: SENSOR CASING LID	
AUTHOR: M. Adriaanse	A4
SCALE: 1:1	SHEET 1:1

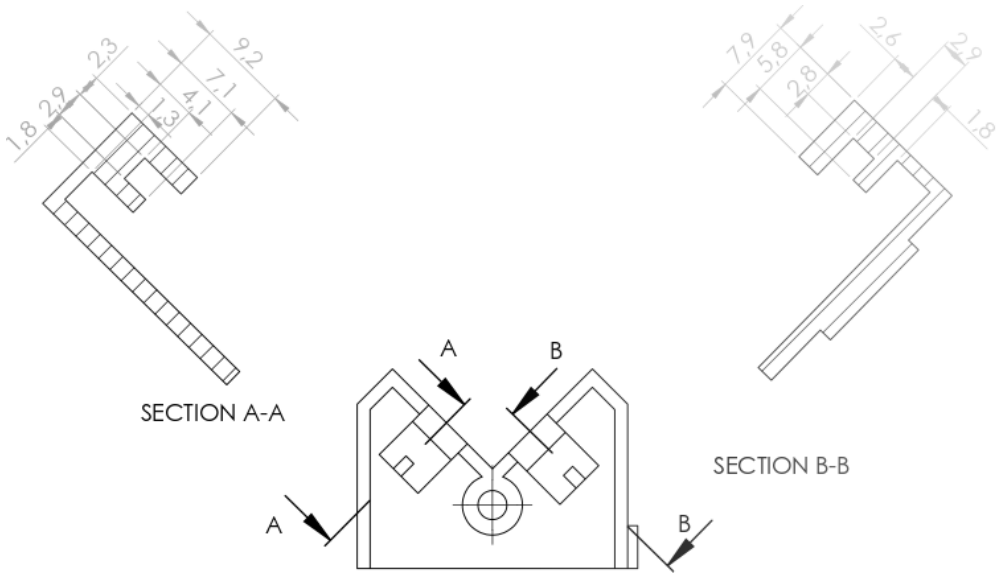

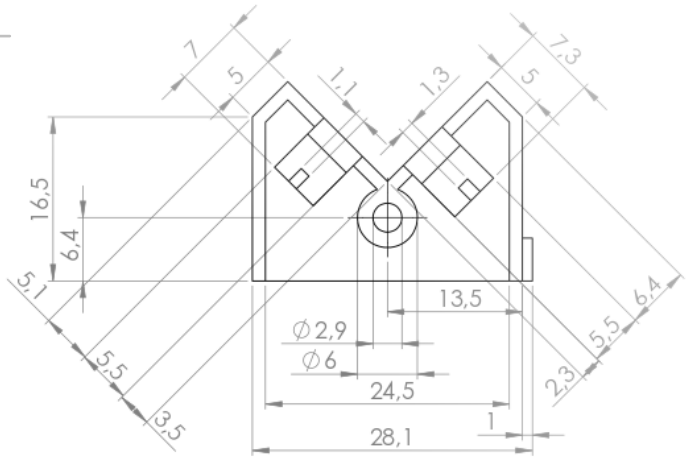

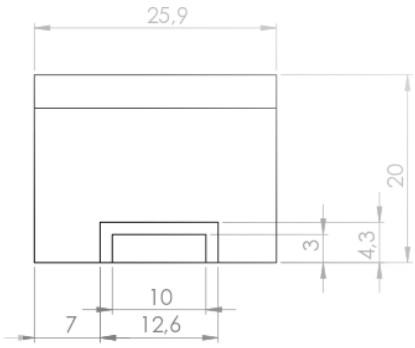

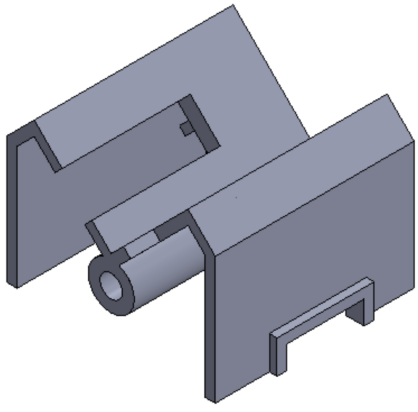

MATERIAL:	PLA BLACK
DIMENSIONS ARE IN MM	
TITLE: SENSOR CASING BODY	
AUTHOR: M. Adriaanse	A4
SCALE: 1:1	SHEET 1:1

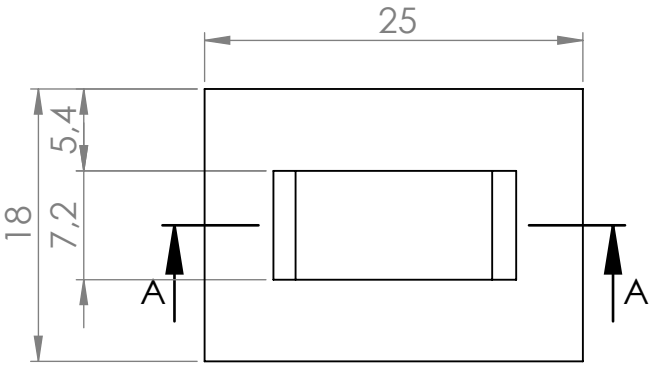

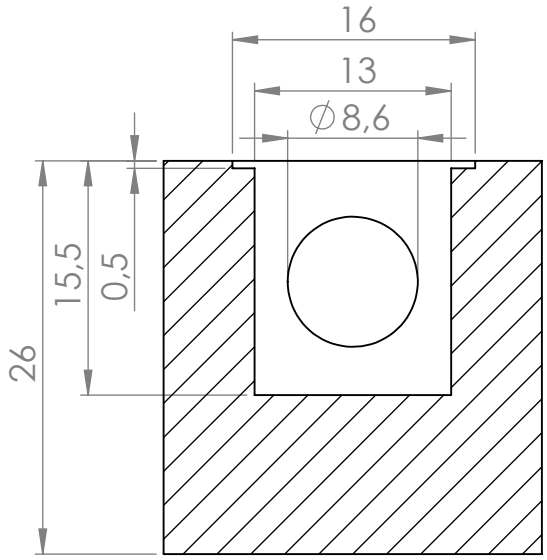

SECTION A-A

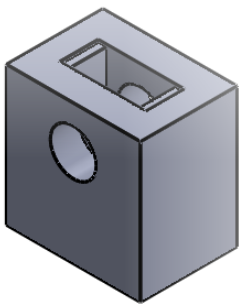

MATERIAL:	PLA BLACK
DIMENSIONS ARE IN MM	
TITLE: Set screw base	
AUTHOR: M. Adriaanse	A4
SCALE: 2:1	SHEET 1:1

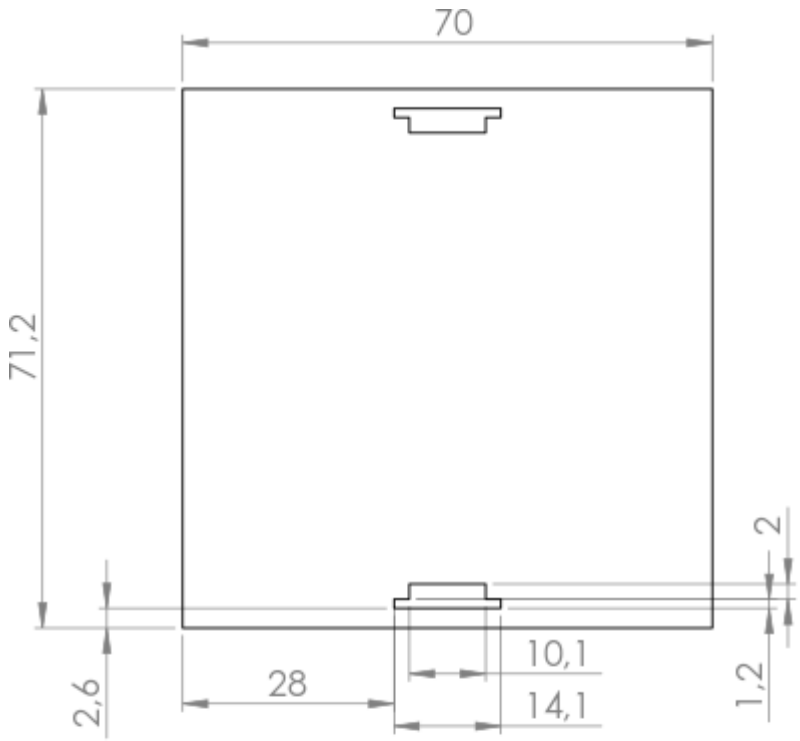

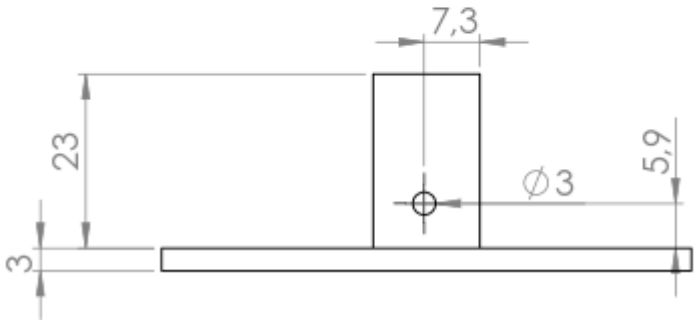

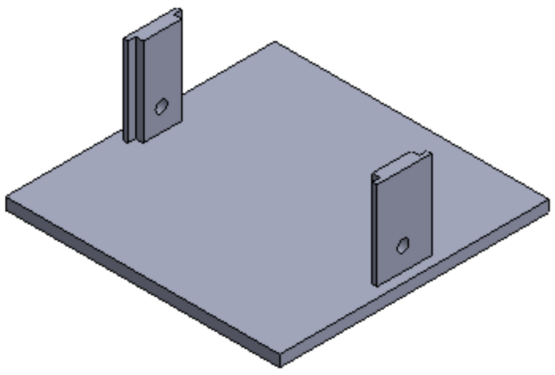

MATERIAL:	PLA BLACK
DIMENSIONS ARE IN MM	
TITLE: LINEAR STAGE BASE	
AUTHOR: M. Adriaanse	A4
SCALE: 1:1	SHEET 1:1

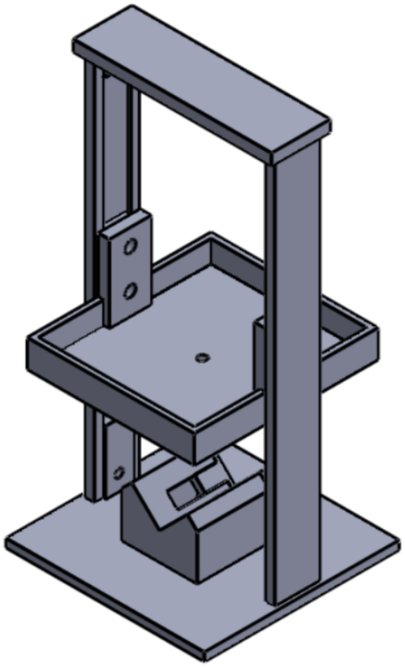

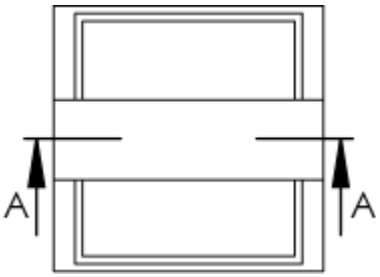

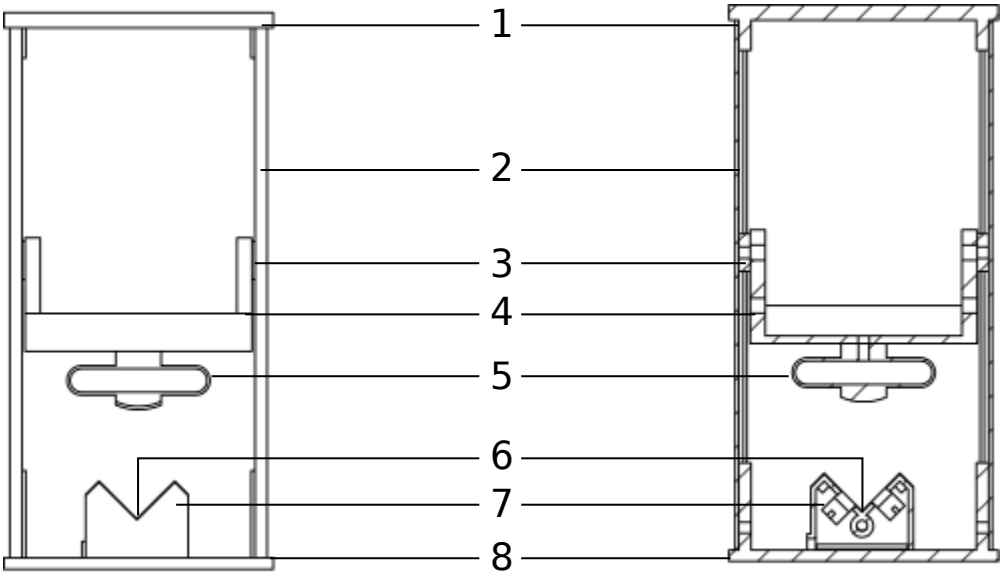

SECTION A-A

Assembly part list	
1	Linear stage top
2	Drylin linear guide
3	Drylin slider
4	Weight holder
5	Weight holder
6	Sensor casing lid
7	Sensor casing body
8	Linear stage base

MATERIAL:	PLA BLACK
DIMENSIONS ARE IN MM	
TITLE: FA-MPA ASSEMBLY	
AUTHOR: M. Adriaanse	A4
SCALE: 1:2	SHEET 1:1

Appendix E - Experiment documentation

This appendix contains the randomized measurement orders, a blank version of the case report form, a blank version of the measurement protocol form, a guide to the distal phalanx measurements and an experimental layout and component list that were used for the experimentation with the FA-MPA.

Measurement order randomization

Table 1 - Measurement order randomization table for FA-MPA contact force measurements.

Measurement order randomization table

Exp. No.	*1*	*2*	*3*	*4*	*5*	*6*	*7*	*8*	*9*	*10*	*11*	*12*	*13*	*14*	*15*	*16*	*17*	*18*	*19*	*20*	*21*	*22*	*23*	*24*	*25*	*26*	*27*
	1	1	1	1	1	1	1	1	1	1	1	1	1	1	1	1	1	1	1	1	1	1	1	1	1	1	1
	3	6	6	7	7	5	7	6	3	7	6	2	6	7	4	7	5	6	2	3	7	6	6	2	6	2	2
	2	3	7	5	2	6	6	7	6	2	5	6	4	2	3	3	7	5	3	5	6	2	3	5	3	6	5
	4	5	3	6	4	7	3	2	7	3	2	7	2	4	7	4	2	4	5	7	4	3	7	4	2	3	4
	5	2	5	3	6	4	2	3	5	6	3	5	7	3	6	6	3	7	4	4	3	7	2	7	7	4	7
	7	4	4	2	3	2	4	4	4	5	4	3	3	6	2	5	6	3	7	2	2	5	5	6	5	5	6
	6	7	2	4	5	3	5	5	2	4	7	4	5	5	5	2	4	2	6	6	5	4	4	3	4	7	3

Table 2 - Translation of force measurement numbers to added weight in the weight holder, total weight on the distal phalanx and approximation of force added on the distal phalanx

Force measurement legend

Table 1 index	Added weight in weight holder (g)	Total added weight on phalanx (g)	Total added force on phalanx (N)
1	0 (without container)	0	0.0
2	30	50	0.5
3	80	100	1.0
4	130	150	1.5
5	180	200	2.0
6	230	250	2.5
7	280	300	3.0

Case report form: FA-MPA measurements cohort 01

Experiment date (DD/MM/YYYY): ___/___/_____

Experiment time (HH:MM): ___: ___

Experiment No.: _____

Data code format (FA01_*Exp.no*:): FA01_ _____

Experimental setup check

Room data:

Location: _____

_____

Room temperature: _____ °C

General subject data

Date of birth (Age): ___/___/___ (_____yrs.)

Biological sex at birth: Male / Female

Length (In passport): _____ cm

Weight: _____ kg

BMI (mass/length^2): _____

Smoker?: No / Yes (quantity:_____)

(Mis-) Use of Medication?: _____

_____

_____

History of CVD?: _____

_____

_____

Base subject measurements

Blood pressure:	SBP _____ mmHg / DBP _____ mmHg
Mean Arterial Pressure:	_____mmHg
Heart rate at rest:	_____BPM
Length left index phalanx (30%):	_____mm (_____mm/_____mm)
Width left index phalanx (at 30%):	_____mm
Height left index phalanx (at 30%):	_____mm

Measurements

Measurement order: M1 ____ ____ ____ ____ ____ ____

Weight on scale during	Measurement 1 (Baseline):	_____g
Weight on scale during	Measurement 2:	_____g
" "	Measurement 3:	_____g
" "	Measurement 4:	_____g
" "	Measurement 5:	_____g
" "	Measurement 6:	_____g
" "	Measurement 7:	_____g

Additional remarks or questions

Protocol form: FA-MPA measurement

This protocol has been written to ensure all measurements into the optimal contact force range between the left distal phalanx of the index finger and the FA-MPA are done in a predetermined, standardized manner. Please ensure that the protocol is followed closely, and all necessary information is given during the corresponding steps. Prior to starting the checklist, fill in the date, time and experiment number. These will form the Data code that is used for data storage and processing.

☐ Determine experiment date, time and number

☐ Reformulate into a Data code and build proper pathway (storage folder) for data collection

---

Experimental setup check

☐ All necessities listed in the document ‘Experimental component list and layout’ present

☐ Setup organized as listed in the document ‘Experimental component list and layout’

☐ Equipment turned on and functionality checked

☐ Register room data

Subject welcome

☐ Seat subject at table and provide (De-) Briefing form

☐ Check if all information is understood and write down remarks

☐ Provide informed consent form

☐ Check if informed consent form is signed

General subject data

☐ Collect all necessary general subject data

☐ Check if all answers are given concisely and to the best of the subject’s knowledge

---

Base subject measurements

☐ Seat subject at setup table

☐ Take blood pressure of subject on the right arm

☐ Determine heart rate at rest

☐ Take fingertip measurements according to the document ‘Distal Phalanx Measurements’

Measurements

For measurement 1: Baseline measurement

☐ Place index finger of subject on 30% length mark according to the document ‘Distal Phalanx Measurements’

☐ Instruct subject to remain still and silent during the measurements

☐ Perform measurement 1 with no weight added for exactly 2 minutes

☐ Note actual weight on scale during measurement

☐ Store data as ‘Data code format‘+_01

☐ Have the subject rest for a couple of seconds

Now, perform the next six measurements according to the predetermined measurement order, in the same manner as measurement 1. THE FOLLOWING CHECKLIST IS THUS NOT NECESSARILY IN THE RIGHT MEASUREMENT ORDER.

☐ Measurement 2:

☐ Note actual weight on scale during measurement

☐ Saved as ‘Data code format’+_02

☐ Rest

☐ Measurement 3:

☐ Note actual weight on scale during measurement

☐ Saved as ‘Data code format’+_03

☐ Rest

☐ Measurement 4:

☐ Note actual weight on scale during measurement

☐ Saved as ‘Data code format’+_04

☐ Rest

☐ Measurement 5:

☐ Note actual weight on scale during measurement

☐ Saved as ‘Data code format’+_05

☐ Rest

☐ Measurement 6:

☐ Note actual weight on scale during measurement

☐ Saved as ‘Data code format’+_06

☐ Rest

☐ Measurement 7:

☐ Note actual weight on scale during measurement

☐ Saved as ‘Data code format’+_07

☐ Rest

Finalization

☐ Check if all data is stored properly and named accordingly

☐ Check if all subject data is gathered on form

☐ Ask if subject has any additional questions. If yes, write down remarks.

☐ Check if all questions answered

☐ Provide with personal copy of (De-) Briefing

End of experiment.

Distal Phalanx measurements

To clarify the measurements to be performed on the Distal phalanx, refer to Figure 1. Fingertip height is measured at the same 15% length as the fingertip width.

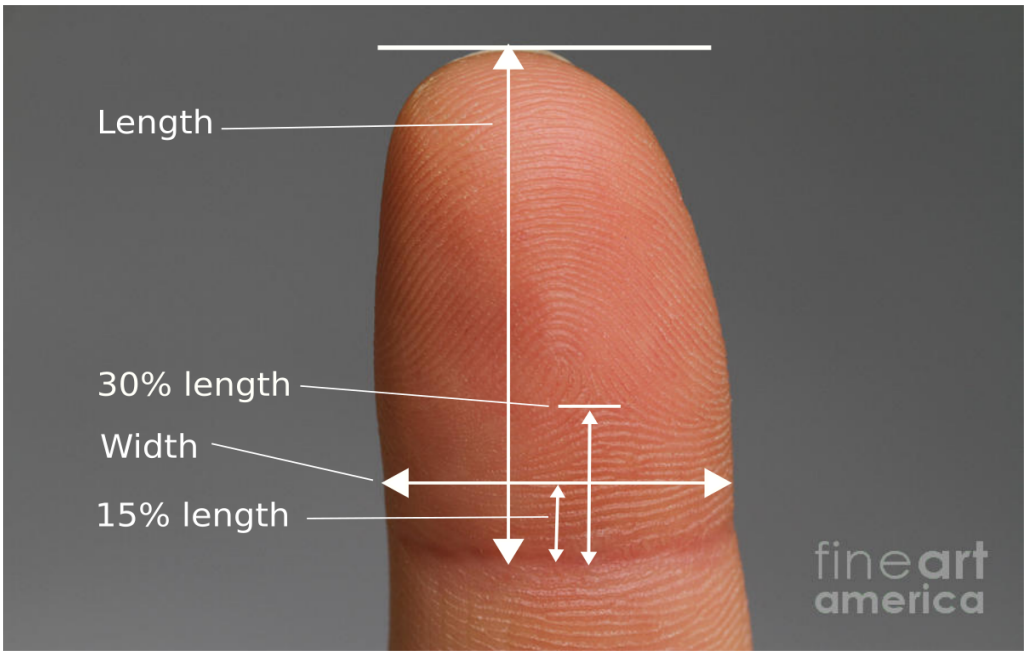

Figure 1 - Clarification of measurement location distal phalanx dimensions

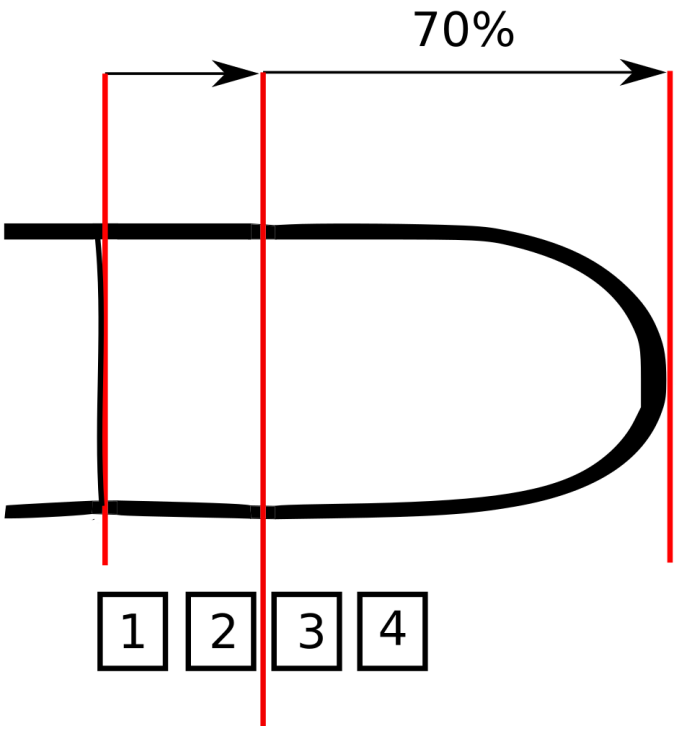

Figure 2 - Placement location of fingertip w.r.t. photodiode array

Experimental setup component list and layout

#	Item (generic)	Item specification of item used	Manufacturer of item used
1	FA-MPA	-	Made in-house
2	Datacable MPA	Datacable FA-MPA specifically made for this prototype	Made in-house
3	Digital signal converter	NI-USB 6211 Multifuction Data Acquisition system	National Instruments, Austin, TX, USA
4	Datacable	USB-B to USB-A	Unknown
5	Laptop	Dell Latitude E6530 with Windows 7 and PWV-calculation programming	Dell inc., Round Rock, Texas, United States
6	Automatic Sphygmomanometer	GE Datex Ohmeda S5	GE Healthcare, Chicago, Illinois, United States
7	Weights	200g – 100g – 50g – 20g - 10g	Hi-Tech
8	Thermometer	Basetech thermometer E0217	Conrad Electronics SE, Hirschau, Germany
9	Stopwatch	Built in Application, Iphone 6, iOS 12.1.2	Apple Inc., Cupertino, California, United states
10	Digital scale	Kern EMB 1200-1	Kern & Sohn, Balingen, Germany
11	Heart rate monitor	Datascope Radical RDS1	Masimo, Irvine, California, United States

Furthermore, make sure all equipment is placed on a table with enough space so the setup is not cramped, and there are two chairs provided for the researcher and subject.

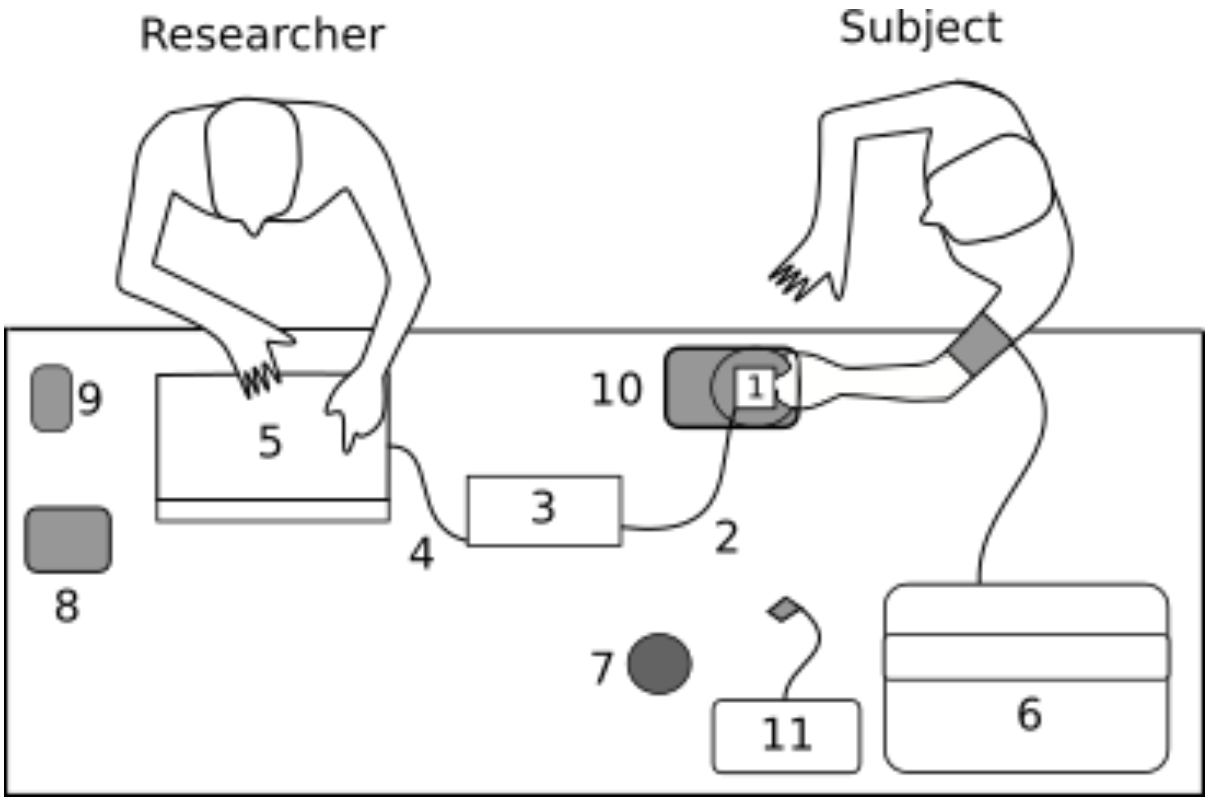

Appendix F - Future recommendations

FA-MPA redesign

The sensor was designed according to the SOR provided in Appendix B, however requirements for sensor size and electrical component modularity are believed to have impacted the structural and electrical integrity of the sensor and to have introduced measurement errors. It is highly recommended to redesign the experimental FA-MPA as a purely experimental sensor, disregarding the size constraints for a portable sensor and preferably using non-modular components, to prevent measurement errors caused by moving parts or faulty electrical contacts. In the future, the knowledge attained about exact during experimentation with a structurally sound senor can be implemented in a miniaturized sensor casing with a modular electrical infrastructure. The linear stage can still be very useful in adding contact pressure between the tissue and the sensor in the future, but it is recommended to implement a force sensor between the sensor casing and baseplate, or to redesign these parts as a single device, to be able to measure real-time contact force instead of having to derive this from the weight measured on a scale. This will allow for the direct coupling of PPG signal and the values for the determined PWV to an exact contact force at that moment, providing a clearer image of the effect of contact force on PWV determination robustness. [APPENDIX C]

FA-MPA rebuild

Fabrication of the experimental sensor encountered technical hurdles, that were only overcome with difficulty. The fabrication of the PD and LED modules proved to be difficult by hand. The contacts were soldered with a generic soldering iron with a small tip, however higher placement accuracy and structural and electrical integrity might be achieved when using solder reflow techniques [1]. This would also open the possibility to shield the conducting elements from outside elements, since it was found that contact between the anode terminal of the diode and the skin of subjects caused a very high frequency signal noise to occur, of which the amplitude was roughly 3 times as high as the amplitude of the PW. The sensor would greatly benefit from a standardized fabrication process, which focuses on structural and electrical integrity of the components, which are preferably also specifically chosen to match with the fabrication technique. This will improve the eventual viability of a modular sensor in which modules are just as reliable as a fixed electrical, non-modular infrastructure. Additionally, the sensor casing should also be redesigned to incorporate the newly designed electrical infrastructure and redesigned for structural integrity and stability, preventing the electrical components from moving. [FORCE SHIELDING AND DESIGNS]

Further experimentation

With improved sensor reliability through fabrication quality, experimentation to further specify the exact range of contact forces for which the PWV determination is robust is highly recommended. The range between 3.43 to 3.92 can be used as a basis from how to choose the range of forces that are tested in the future, but as the test measurement at 450g showed, there is believed to be a maximum force for which the PWV determination is still robust. 7 test measurements were performed to provide an image as to what future experiments could entail. In measurement 1, PPG signal was retrieved when an excessive force was applied to the distal index phalanx. In the other measurements, the intermediate instead of the distal phalanx was lined up with the PD array. In measurement 3 and 4, the intermediate phalanx of the middle finger was used and in measurement 6 and 7 the intermediate phalanx of the index finger was used while the finger was not fully outstretched, but there was a slight bend between the proximal and the intermediate phalanges to possibly relieve stress in the tissue due to tendon stress. The results of these test measurements are shown in **Table 1**. During measurement one, wave shapes were either barely visible or heavily distorted, leading to a very low value for PWQR. Measurements 5 and 6, where the intermediate phalanx was lined up to the PD array instead of the distal phalanx both show very good results in terms of high PWQR, low PWV variance and realistic Mean Median PWV values. Therefore it is recommended to seek out additional placement options on the hand other than the distal phalanx of the index finger. Other locations of placement would require future researchers to think about comfort and implementation because the technique of the MPA is not merely added to the existing fingertip saturation meters anymore.

Table 1 - Results for seven test measurements under varying conditions. $F_{contact}$ = contact force between the tissue and the sensor surface. The bend during measurement 6 and 7 was approximately 90 degrees and remained static during the measurement.

#	Digit	Phalanx	Alignment	Heartbeats measured	$F_{Contact}$ [N]	PWQR	Mean med. PWV [m/s]	PWV variance [m/s]
1	Index	Distal	Straight	79	4.41	-0.56	-	-
2	Index	Intermediate	Straight	33	3.53	1.00	2.02	11.29
3	Index	Intermediate	Straight	31	4.07	1.00	3.78	6.49
4	Middle	Intermediate	Straight	31	4.32	1.00	1.73	54.03
5	Middle	Intermediate	Straight	25	4.91	0.93	1.16	0.16
6	Index	Intermediate	Bent	23	2.65	0.62	-1.68	0.76
7	Index	Intermediate	Bent	23	3.92	1.00	0.76	0.01

Implementation feasibility

It is highly recommended to investigate the actual feasibility of implementation of a sensor for PWV determination in the peripheral vasculature for two main reasons: First off, inferred from Hagen-Poisseuilles law for laminar flow, the assumption that is made for the Moens-Koreweg equation that the fluid is inviscid does not apply for smaller arteries of the peripheral vasculature [2]. Therefore the actual relationships between the arterial blood pressure, PWV and arterial stiffness in the peripheral vasculature should be further investigated and quantified to investigate the actual prognostic value of PWV determination in the peripheral vasculature. The Hagen-Poisseuille law is shown in Eq. (1), where ΔP is the pressure difference over the length of the flow trajectory in Pascal, μ is the blood viscosity, L is the length of the trajectory in meters, Q is the fluid volume flow in cubic meters per second and R is the radius of the artery.

$$\Delta P = \frac{8\mu LQ}{\pi R^4} \ [Pa] \qquad \text{Eq. (1)}$$

Reason two is the tenacious presence of movement and positioning artifacts when the sensor is to be placed on the distal phalanx according to both this study and that of van Velzen [3]. Successful implementation would require that the absolute 'sweet spot' for sensor positioning and contact force was found in combination with a design that absolutely eliminates all movement artifacts of the sensor, which presumably would deteriorate comfort.

Sensor multifunctionality and clinical relevance

With improved sensor reliability through fabrication quality, sensor multifunctionality is an interesting development field to enhance the clinical relevance of an MPA-based sensor. Exploring possibilities for heart rate monitoring and pulse oximetry to be added functionalities for the MPA-based sensor could help make the implementation of the sensor easier due to the technique of PWV measurement being incorporated in an already commonly used sensor, the pulse-oximeter clip. Alternatively, might the relation between peripheral PWV and arterial stiffening not be substantiated, the technique of measuring PW propagation could be used for tracing irregularities in superficial vascular tissue, which could prove useful in the treatment of superficial arterial occlusion [4]. This technique could even be extended to the tracing of occlusion or arterial irregularities inside the body, where intervention techniques are too risky and percutaneous catheterization is difficult.

To summarize: It is recommended to redesign and rebuild the FA-MPA as a whole, focusing on structural and electrical integrity to improve measurement reliability. The results of a newly designed study are to be translated into a clinically implementable device, of which the clinical relevance and feasibility has been investigated.

References

1. Yang, D. 2018 [cited 2019 23-04]; Available from: https://www.techbriefs.com/component/content/article/tb/features/articles/28337?start=1.
2. Sucowsky, P. *Cardiovascular Biofluid Mechanics Chapter 4: Mathematical Modeling*. 2016 [cited 2019 25-05-19]; Available from: http://www.wright.edu/~philippe.sucosky/ME7370.html.
3. van Velzen, M.H.N., *The Speed Of Waves - Measuring the velocity of pressure pulse waves traveling through blood in the peripheral blood vessels*. 2019, Erasmus Universiteit Rotterdam.
4. Allen, J., et al., *Photoplethysmography detection of lower limb peripheral arterial occlusive disease: a comparison of pulse timing, amplitude and shape characteristics.* Physiol Meas, 2005. **26**(5): p. 811-21.